Solid-state nanopore sensors

Liang Xue[1,4], *Hirohito Yamazaki*[2,3,4], *Ren Ren*[1], *Meni Wanunu*[2]✉, *Aleksandar P. Ivanov*[1]✉ *and Joshua B. Edel*[1]✉

Abstract | Nanopore-based sensors have established themselves as a prominent tool for solution-based, single-molecule analysis of the key building blocks of life, including nucleic acids, proteins, glycans and a large pool of biomolecules that have an essential role in life and healthcare. The predominant molecular readout method is based on measuring the temporal fluctuations in the ionic current through the pore. Recent advances in materials science and surface chemistries have not only enabled more robust and sensitive devices but also facilitated alternative detection modalities based on field-effect transistors, quantum tunnelling and optical methods such as fluorescence and plasmonic sensing. In this Review, we discuss recent advances in nanopore fabrication and sensing strategies that endow nanopores not only with sensitivity but also with selectivity and high throughput, and highlight some of the challenges that still need to be addressed.

The ability to detect single molecules has resulted in extraordinary advances in science and medicine. Ever since Richard Feynman envisaged the rise of nanotechnology and the possibility of manoeuvring objects atom by atom in his landmark talk in 1959 (REF.[1]), there has been a drive not only to use this capability to control the properties of materials but also to better understand molecular behaviour and interactions. For example, observing and studying molecules one at a time unleashes new prospects for probing fundamental dynamic processes that take place at the interface of life sciences, biophysics, chemistry and medicine[2–4]. Whereas the majority of conventional experimental techniques yield information that is time-averaged and population-based, single-molecule measurements allow us to probe how individual members of a molecular population behave and interact, resolving the structural and spatial dynamics. Probing a single molecule, the equivalent of 1.66 yoctomoles, necessitates sensitive methods that amplify the measurement signal, such as the photon flux emitted from a single dye or, in the case of traditional nanopore sensors, the residual ion flux passing through a molecule as it transiently occludes the pore volume.

Over the years, several detection strategies sensitive enough to detect single molecules were developed, including scanning-probe methods, such as atomic force microscopy[5,6] and scanning tunnelling microscopy[7,8] (STM). Such instrumentation is not only capable of atomic resolution but can also be used to perform nanoscale surface analysis to extract chemical, electrical and even mechanical properties of single molecules. For the detection of single molecules in liquids, optical methods have been in widespread use since the first visual observation of individual molecules in 1976 (REF.[9]). More recently, label-free, electrical-based methods have been gaining prominence, in large part owing to improvements in devices and detection methods, enabling the design of sensors with dimensions comparable to those of a molecule[3,10,11]. One example is ionic current detection using nanopore sensors (BOX 1). The foundations of this method can be traced back to the use of Coulter counting to count and size particles suspended in electrolytes in the 1950s and to the introduction of single-channel current recording in the 1970s, for which Erwin Neher and Bert Sakmann were jointly awarded the 1991 Nobel Prize in Physiology or Medicine. However, it was only in the late 1990s that the idea of using nanopores gathered critical momentum, largely fuelled by the ambitious goal of using them for next-generation nucleic-acid sequencing[12]. It took less than two decades for the first sequence reads of DNA strands using nanopores to be published[13]. Subsequently, commercialization of the nanopore-sequencing technology by Oxford Nanopore Technologies sparked a wide range of applications and stimulated interest beyond the nanopore community[14,15]. Today, nanopore sensing is rapidly advancing not only in the context of DNA sequencing but also for other applications, such as biological screening, diagnostics[16–18] and the grand challenge of protein sequencing[19,20].

At the core of every single-molecule method is the necessity to confine individual analytes in space and time during the measurement. Ideally, the dimension of the sensing volume should be comparable to the size of the analyte to achieve single-molecule sensitivity[3,10,21]. In traditional optical methods, a 'virtual' volume often defines a region within which molecules can be detected.

[1]*Department of Chemistry, Imperial College London, Molecular Sciences Research Hub, London, UK.*

[2]*Department of Physics, Northeastern University, Boston, MA, USA.*

[3]*Department of Biological Sciences, Graduate School of Science, The University of Tokyo, Tokyo, Japan.*

[4]*These authors contributed equally: Liang Xue, Hirohito Yamazaki*

✉*e-mail: wanunu@neu.edu; alex.ivanov@imperial.ac.uk; joshua.edel@imperial.ac.uk*

https://doi.org/10.1038/s41578-020-0229-6

Box 1 | **How nanopores work**

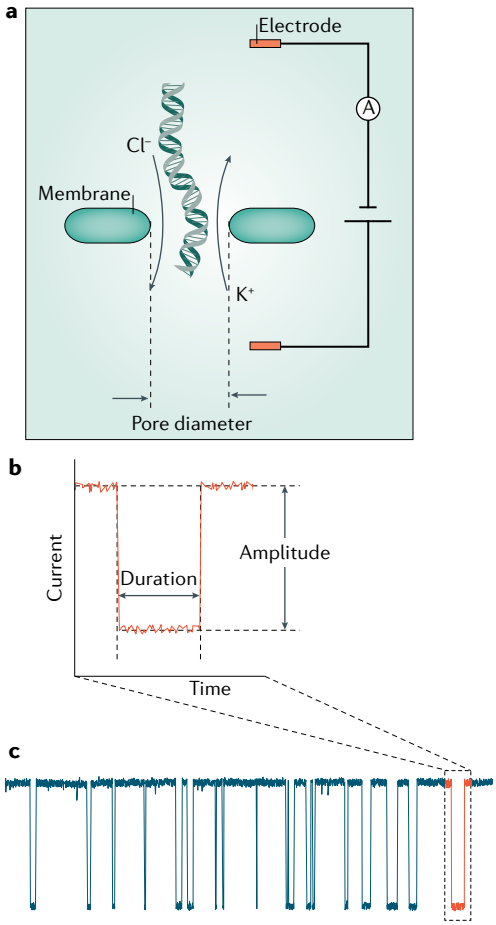

The principle behind conventional nanopore detection is resistive pulse sensing. Two reservoirs filled with an electrolyte (usually a buffered salt solution such as KCl, NaCl or LiCl) are separated by a thin, non-permeable membrane and linked via a single nanopore. Electrodes, for example, Ag/AgCl, are immersed in the two compartments (panel **a** of the figure) and a constant voltage bias is applied across the nanopore (that is, the voltage is clamped), causing a steady-state ionic-current flux through the pore. During the passage of an analyte through the pore (often dubbed translocation), the ionic current usually decreases owing to hindered access of ions to the pore volume[345,346]. In some cases, such as for double-stranded DNA transport in solutions with a low salt concentration, recruitment of mobile counterions by the DNA backbone near the pore enhances the ionic current instead. Other factors, such as salt concentration and pH, can influence the interplay between the electrophoretic and electro-osmotic flow. By analysing the features of the current pulse, such as its amplitude, duration and noise (panel **b** of the figure), one can obtain important information on the analyte, including its size[26], charge[283], affinity with the nanopore surface[170] and, in some cases, even its shape[149], dipole moments[150] and sequence[79]. Additionally, the frequency of these modulations carries information on the analyte concentration (panel **c** of the figure).

By contrast, in nanopores, a molecule is confined in a physical volume. One requirement is that the diameter of the nanopore is similar to that of the molecule to facilitate detection. At the same time, the nanopore depth or thickness should be as small as possible to maximize the detected signal. Many challenges had to be overcome to reach the present state of the technology, which required improving the tuning of the material properties, dimensions, selectivity and detection modality.

In this Review, we start by surveying recent advances in the use of a range of different materials, including proteins[22,23], silicon[24,25], quartz[26,27], metals[28,29], polymeric films[30,31], nanowires[32] and 2D materials such as graphene[33,34], to make nanopores. We explore how these materials are enabling novel sensing functionalities and highlight recent solutions to one of the greatest drawbacks associated with nanopore sensing: the lack of selectivity. We discuss recent strategies to achieve the much-needed analyte selectivity via chemical modification of the nanopore material or modification of the way analytes are transported through the nanopore. Finally, we touch on areas of research that aim to capitalize on the advantages of coupling nanopore sensing to other detection modalities, including field-effect transistors (FETs), quantum tunnelling and optical detection. The emerging incorporation of machine-learning algorithms with nanopore sensing to facilitate data analysis is also discussed. This article provides a glimpse into the state of the art in nanopore sensing from a materials perspective. Specifically, we focus our discussion on the use of solid-state pores and only introduce biological pores when necessary. We refer the reader to other reviews[10,35] for a discussion of the achievements and challenges associated with biological nanopores.

Overall, nanopore sensing has great potential, but important challenges lie ahead. From a materials perspective, there is a drive to invent novel nanopore architectures and materials, and achieve multiplexed detection, high-throughput analysis, enhanced sensitivity and selective and/or specific detection. Apart from DNA and RNA sequencing, the chances of clinical adoption of nanopore technologies are high, but most likely they will require more complex signals than ionic currents alone. This is, in part, due to the need to detect small molecular differences in complex diagnostic biofluids such as serum, cerebrospinal fluid and urine. Such measurements often require the use of a 'spectroscopic' fingerprinting approach rather than the more typical 1D signals obtained with nanopores. We hope to convey to the reader that there is much to be gained by incorporating additional detection modalities into nanopores.

Materials and fabrication methods

Nanopore fabrication and membrane thinning. The nanopore geometry is a major contributor to the overall measurement sensitivity. There are a number of tools available to define and optimize the diameter, thickness and profile of the pore, including focused electron/ion beams[36–41], controlled dielectric breakdown (CDB)[42–47], laser pulling of glass or quartz pipettes[48–52], electrochemical deposition[53,54], nanoimprinting[55], thermal annealing[56–58], chemical etching of membranes with nucleated defects[59–61], hard masks[62–64] and metal catalysts[65,66] (TABLE 1). For an in-depth explanation of each nanopore-fabrication technique, the reader is referred to alternative reviews[47,67–69]. Methods for fabricating pores in the sub-10 nm range are the most attractive for high-resolution discrimination between different molecular building blocks, such as nucleotide bases and amino acids. Focused electron/ion-beam-induced pore fabrication is perhaps the most commonly used approach in the sub-10 nm range, as the pore size and shape can be tuned at a designated location by controlling the beam spot size, dwell time and position on the membrane[70,71] (FIG. 1a). Furthermore, it is possible to monitor the pore size in real time during the fabrication process, which is important when it comes to making size-reproducible pores[37,72]. Considerable drawbacks are instrumentation availability, cost and the fact that the pores are fabricated under ultra-high vacuum conditions (10^{-4}–10^{-9} Pa), which can result in a change in geometry when the pores are exposed to the hydrated environment they are meant to work in. CDB is another

method that is gaining prominence: in CDB, nanopores are fabricated directly in solution and at a lower cost by applying a voltage across the membrane[42,47] (FIG. 1b).

The thickness of the membrane is critical to optimize detection, as the signal (the ionic-current amplitude) and the resolution (the effective sensing length in the nanopore) scale, to a first approximation, inversely with pore thickness. Therefore, there has been a drive to create nanopores at the ultimate limit: a single-atom-thick membrane. However, atom-thick nanopores are exceptionally challenging to realize, as the membrane often becomes brittle.

Over the past decade, multiple approaches have been developed to fabricate atomically thin membranes (TABLE 2). A widespread strategy for achieving single-digit nanometre thickness is based on the thinning of existing solid-state membranes. For example, a silicon nitride (SiN) membrane, which is commonly used as a hard mask in silicon wafer processing, can be selectively etched using either a dry-etch process[73] (FIG. 1c), electron/ion-beam irradiation[36,74,75] (FIG. 1d) or laser-assisted photothermal etching on a selected area of the sample[76,77] (FIG. 1e). Following the thinning step, a pore can be fabricated by either focused electron/ion beam[36,37,74] or CDB[42]. When CDB is combined with laser-assisted photothermal etching[77] or dielectric breakdown etching[78], a nanopore with a short channel (~1 nm) can be fabricated in a fluidic cell without the need for aggressive chemical cleaning (FIG. 1f).

A second fabrication strategy involves the deposition of an ultra-thin membrane using atomic layer deposition (ALD) on a sacrificial layer that is then removed, resulting in a thin, free-standing membrane with a desired composition, such as SiO_2 (REF.[79]), TiO_2 (REFS[80,81]), Al_2O_3 (REFS[82–85]), nanoporous Al_2O_3 (REF.[86]), graphene–Al_2O_3 (REF.[87]) and HfO_2 (REFS[88,89]) (FIG. 1g). This approach is complementary to the more typical use of ALD and chemical vapour deposition (CVD) coatings to either modify the pore surface or control the pore diameter[77,90–93]. The advantage of using ALD is that the membrane thickness can be finely controlled by choosing appropriate deposition cycles. For example, a deposition rate of 1.4 Å per cycle was used to obtain a HfO_2 membrane with a target thickness of 4.5 nm (REF.[88]). ALD can be further used to deposit thin multilayers of different materials[77,92]. The use of different materials

Table 1 | **Pore-fabrication techniques**

Fabrication technique		Advantages	Disadvantages	Pore size (nm)	Refs
Focused electron/ion beams	Transmission electron microscope (TEM)	Tuning pore size and shape at a designated location by controlling the beam spot size, dwell time and position. Real-time monitoring of the pore size during fabrication	Pore geometry in hydrated condition can be different from that in vacuum. Pore surface can be hydrophobic owing to hydrocarbon contamination. High-energy beam instrument (TEM or FIB) is required	>0.13	37,40,41, 70–72
	Focused ion beam (FIB)			>1.8	36,38, 39,74
Controlled dielectric breakdown		In situ nanopore fabrication using only a voltage–current reading apparatus, no pore cleaning or wetting required	Possible formation of multiple nanopores at the same time. No control on the pore location unless additional methods are used (plasmonic nanostructures, laser etching, atomic force microscopy tips)	>1.1	42–47,314
Laser pulling of glass or quartz pipettes		Quick and low-cost fabrication. Compatible with scanning-probe-microscopy methods. Straightforward fabrication of closely spaced groups of two or four nanopores using multi-barrelled pipettes	Sub-10 nm pore fabrication is challenging. Requires a pipette puller	>4.7	27,48–52
Electrochemical deposition		In situ shrinking. Possibility of fabricating nanopores with an embedded gate electrode.	Requires pre-pore fabrication of the electrode-integrated membrane and results in larger nanopores. Requires optimization of the deposition conditions	>8	53,54
Nanoimprinting		Quick and low-cost fabrication of nanopore arrays	Works only with polymeric membranes	>6	55
Thermal annealing		Fabrication of nanopore arrays	Requires high temperature (>1,000 °C) with precise control using a furnace or laser. Long etching time. Local heaters (such as gold nanoparticle) have to be dispersed	>2	56–58
Chemical etching	With nucleated defects	Fabrication of nanopores in membranes with micrometre or nanometre thickness	Requires heavy ion irradiation and an accurate etching profile. Long etching time. Challenging to control the number of pores	>2	59–61
	With hard masks		Requires patterned mask deposition and an accurate etching profile. Long etching time	>5	62–64
	With metal catalysts		Requires nanoscale metal deposition and an accurate etching profile. Long etching time	>20	65,66

diversifies the range of surface properties of the membrane, which can be useful to tune the interaction with specific analytes. In particular, HfO_2 membranes facilitate reduced pore degradation and slow DNA translocations owing to a physicochemical interaction with nucleic acids[88]. ZnO (REF.[94]) and Al_2O_3 (REF.[84]) membranes display enhanced attractive electrostatic interaction with negatively charged DNA. Reducing the

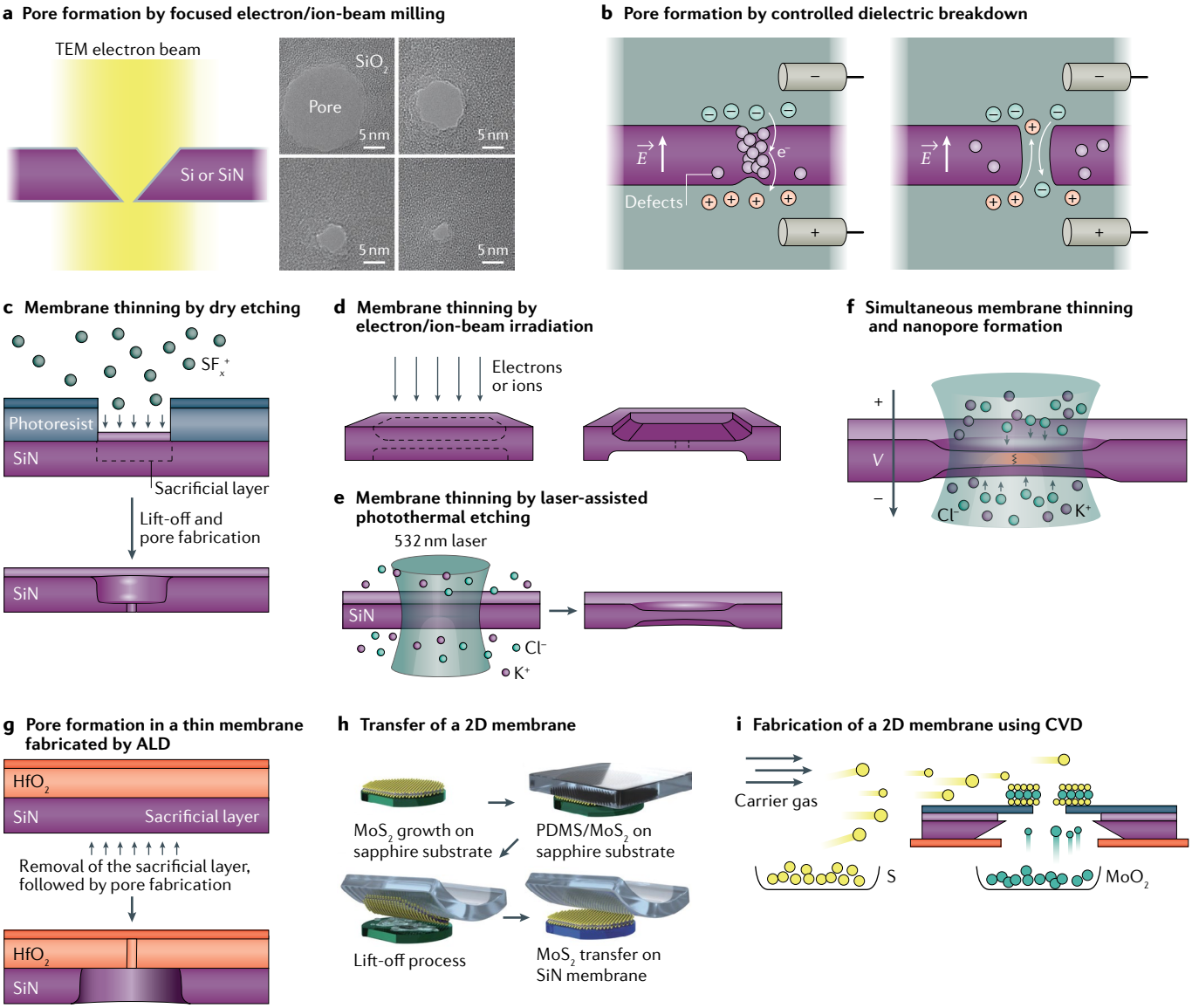

Fig. 1 | **Methods of fabricating small and thin nanopores. a** | Focused electron/ion-beam milling of free-standing membranes is a common approach for fabricating sub-10 nm pores (left). The pore size and shape can be monitored in real time during fabrication. A sequence of transmission electron microscope (TEM) images showing nanopore formation in silicon dioxide using an electron beam (right). The electron irradiation leads to a gradual reduction in the size of the nanopore to approximately 3 nm. **b** | Controlled dielectric breakdown can be used to fabricate pores in membrane materials such as SiN, HfO_2 and SiO_2. The membrane is immersed in an electrolyte (such as KCl, NaC or LiCl) and exposed to an electric field with intensity comparable to the dielectric strength of the membrane. Structural defects are produced owing to tunnelling leakage current, resulting in the dielectric breakdown of the membrane and in the formation of a nanopore. **c**–**e** | Thinning methods for solid-state membranes include dry etching with a patterned protection layer (photoresist) (panel **c**); electron/ion-beam irradiation (panel **d**). Helium ion-beam irradiation leads to thinning of both sides of the SiN membrane, which has been attributed to fluidization and ion pressure; laser-assisted photothermal etching (panel **e**). The process is influenced not only by the laser illumination but also by the composition of the supporting electrolyte. **f** | The combination of laser-assisted photothermal etching and controlled dielectric breakdown allows for the simultaneous thinning of the membrane and formation of a nanopore. **g** | Formation of an ultra-thin membrane using atomic layer deposition (ALD). A thin layer of a desired material is deposited on a sacrificial layer using ALD. Etching or removal of the sacrificial layer produces a thin, free-standing membrane; there is a large choice of available deposition chemistries. **h**,**i** | Free-standing 2D membranes. 2D materials supported on a sub-micrometre-sized aperture can be prepared via material transfer (panel **h**) or by directly fabricating the 2D material on the aperture using chemical vapour deposition (CVD) (panel **i**). Nanopores in single-layer 2D materials have high sensitivity, owing to their near-atomic thickness (graphene: 0.3 nm, BN: 1.1 nm, MoS_2: 0.8 nm and WS_2: 0.7 nm). PDMS, polydimethylsiloxane. Panel **a** adapted from REF.[37], Springer Nature Limited. Panel **b** adapted from REF.[42], CC BY 4.0. Panel **d** adapted from REF.[74], CC BY 3.0. Panels **c**, **e** and **f** adapted with permission from REF.[77], American Chemical Society. Panel **h** adapted with permission from REF.[342], Wiley. Panel **i** adapted with permission from REF.[108], American Chemical Society.

Table 2 | **Methods to control pore geometry in thin membranes**

Membrane material	Membrane-preparation method	Pore-fabrication method	Pore thickness (nm)	Pore size (nm)	Analyte	Comments	Refs
SiO_2	Electron/ion-beam irradiation	Focused electron/ion beam	>10	>2	dsDNA	–	37,315,316
	ALD followed by removal of a sacrificial layer	Focused electron/ion beam	>20	>2.5	dsDNA, dsDNA–protein complexes	–	79
	Thermal growth followed by removal of a sacrificial layer	CDB	>30	>5.2	dsDNA	Pore formation on the vertex area of a SiO_2 pyramidal membrane	97
SiN	Dry etching	Focused electron/ion beam	>1.7[a]	>0.8	dsDNA, ssDNA, miRNA, tRNA, dsDNA–protein complexes, proteins, peptides	–	73,271,275, 301,312, 317–321
	Electron/ion-beam irradiation	Focused electron/ion beam	>0.5[a]	>0.9	dsDNA, ssDNA, proteins	Membrane thinning and pore fabrication realized in a single step	25,36,37, 75,174, 322,323
		CDB	>10	>5.2	dsDNA	Pore formation at a thinned region	324
	Dielectric breakdown etching	CDB	>7.52	>11.4	dsDNA	Two-step breakdown using voltage profiles for thinning (constant high voltage) and pore formation (voltage pulse)	78
	Laser-assisted photothermal etching	CDB	>0.5[a]	>1.2	dsDNA, ssDNA, tRNA, proteins	Formation of conical pores at a thinned region	76,77,278
HfO_2	ALD followed by removal of a sacrificial layer	Focused electron/ion beam	>4.5	>1.4	dsDNA, ssDNA	High chemical stability/physicochemical interactions between HfO_2 and nucleic acids	88,89
		CDB	>10	>7	No tested analytes	Pore formation on the vertex area of a HfO_2 pyramidal membrane	96
Al_2O_3	ALD followed by removal of a sacrificial layer	Focused electron/ion beam	>40	>1	dsDNA, dsDNA–protein complexes	Positive surface charge at pH 7–8, nanocrystallites formed at the nanopore surface during focused electron/ion-beam illumination	83,84,87
ZnO	ALD followed by removal of a sacrificial layer	Focused electron/ion beam	>6	>1.3	dsDNA	Positive surface charge at pH 7–8	94
TiO_2	ALD followed by removal of a sacrificial layer	Focused electron/ion beam	>15	>3.1	dsDNA, polypeptides	Low membrane photoluminescence	81
		CDB	>15				
Graphene	Transfer on the aperture	Focused electron/ion beam	>0.3	>3.1	dsDNA, ssDNA, proteins	Hydrophobic interaction between graphene and DNA	80,98,99, 102,154, 325–327
		Electrochemical etching	>0.6	>2.2	dsDNA		117
	Direct growth on the aperture	Focused electron/ion beam	>8	>6.5	dsDNA		100
BN	Transfer on the aperture	Focused electron/ion beam	>1.1	>1	dsDNA, ssDNA	–	104–106,328
MoS_2	Transfer on the aperture	Focused electron/ion beam	>0.8	>0.6	dsDNA, ssDNA, plasmid DNA, nucleotides	–	107,113, 120,305, 328,329
		Electrochemical etching	>0.7	>1	Plasmid DNA	Pore fabrication with sub-nanometre precision using an electrochemical reaction	118
	Direct growth on the aperture	Focused electron/ion beam	>0.8	>2.3	ssDNA	Scalable fabrication of wafer-size, free-standing MoS_2 membranes	108,112

Table 2 (cont.) | **Methods to control pore geometry in thin membranes**

Membrane material	Membrane-preparation method	Pore-fabrication method	Pore thickness (nm)	Pore size (nm)	Analyte	Comments	Refs
WS_2	Transfer on the aperture	Focused electron/ion beam	>0.7	>2	dsDNA	A visible laser can be used to control the nanopore size at the atomic level	109
MXenes	Transfer on the aperture	Focused electron/ion beam	>0.6	>3	dsDNA	Transfer of self-assembled flakes at a liquid–liquid interface	111
Polymerized polyurea	Transfer on the aperture	Focused electron/ion beam	>10	>4	dsDNA, proteins	Hydrophobic surface and a highly negative surface charge density	330

ALD, atomic layer deposition; BN, boron nitride; CDB, controlled dielectric breakdown; dsDNA, double-stranded DNA; ssDNA, single-stranded DNA; miRNA, microRNA; tRNA, transfer RNA. [a]Effective thickness estimated by equations using open-current and ion-current blockade of molecular translocation[73]

membrane photoluminescence by replacing SiN with SiO_2 (REFS[79,95]), Al_2O_3 (REF.[86]) or TiO_2 (REF.[81]) enhances the optical sensitivity for single-fluorophore detection (as discussed in the section on photon-based sensing). The majority of nanopores using membranes fabricated by ALD are made using focused electron/ion beams, and there are only limited reports on pores made by CDB (reported for HfO_2 (REF.[96]), SiO_2 (REF.[97]) and TiO_2 (REF.[81])).

Atomically thin 2D membranes. Nanopore detection using atomically thin 2D membranes was first demonstrated in 2010 using free-standing graphene sheets, ranging from single to a few layers[80,98,99]. Subsequently, sub-nanometre-thick free-standing membranes of several 2D materials have been reported, including graphene[100–103], boron nitride (BN)[104–106], molybdenum disulphide (MoS_2)[107,108], tungsten disulphide (WS_2)[109], bismuth telluride (Bi_2Te_3)[110] and transition-metal carbides (MXenes)[111]. There are two dominant methods used for fabricating free-standing 2D membranes: transfer of a 2D material prepared by exfoliation[110,111] or CVD[80,98,99,103–106,109,112] on a membrane with a relatively large sub-micrometre aperture (FIG. 1h); or growth of the 2D material directly on the aperture using CVD[100,108] (FIG. 1i). The first method is more common, as the procedures for material transfer are well established and the system is easy to inspect optically[113]. Direct CVD grown on the aperture is scalable to whole wafers[108], but the process is challenging to control. In 2D materials, similarly to conventional membranes, the nanopores are typically fabricated using focused electron/ion beam[80,98,99,103–106,109,114–116]. However, other approaches, including electrochemical etching[117,118], photo-oxidation[56,109] and plasma etching[119], have also been used. Nanopores in 2D materials offer high detection sensitivity. For example, all four types of 30-mer polynucleotides and single nucleotides could be identified using a pore with a diameter of 2.8 nm in an atomically thin MoS_2 membrane[120].

Influence of the material on the current noise. The noise in the electrical current is an important factor in nanopore sensing with high temporal resolution; the underlying theory and a comparison between platforms can be found in recent reviews[67,121,122]. From a materials perspective, the noise at high frequencies (>1 kHz) is dominated by the capacitance of the material, as can been seen in the equations defining the dielectric and amplifier noise:

$$S_{\text{dielectric}} = 8\pi k_B T D f C_{\text{material}} \quad (1)$$

$$S_{\text{amplifier}} = (2\pi f v_n C_{\text{total}})^2 \quad (2)$$

where k_B is the Boltzmann constant, T the temperature, D the dissipation factor, f the frequency, v_n the input voltage noise, C_{material} the chip material capacitance and C_{total} the total capacitance, which includes the contributions of the chip material, electrode wiring and amplifier input/feedback elements[123,124]. The material capacitance can be reduced by passivation with polydimethylsiloxane[125] or by using low-capacitance materials, such as amorphous glass[103,126,127], Pyrex[95], polyimide[128] and sapphire[129], as a support substrate instead of crystalline silicon. At low frequencies (<100 Hz), $1/f$ noise dominates. This type of noise is associated with many physical phenomena in sensing systems[130], including surface contamination[131], surface charge fluctuation[132], nanobubble nucleation[133,134], reversible ion absorption at the pore surface[135], poor hydrophilicity of the pore surface[136], mechanical vibration of 2D membranes[80,99,106,137,138] and fluctuation of charge carriers at the Ag/AgCl electrode interface[139].

Chemically dressing nanopores

Surface-modification strategies. The chemical composition of the nanopore is critical to the translocation process and strongly influences factors such as pore–analyte surface interaction, receptor binding and electro-osmotic flow. There is an arsenal of chemical-functionalization strategies that can be used to tailor the surface properties. For example, nanopores made from silicon nitride or glass can be functionalized using a large library of silane chemistries, whereas nanopores based on metallized (for example, gold) membranes can be modified using thiol chemistry via vapour or solution-based deposition[140,141].

While many solid-state materials have well-defined properties such as surface charge, they typically do not contain functional groups such as carboxylic acids and amines, unlike biological membranes. To better mimic

biological analogues, various surface-modification strategies have been developed. Examples include the use of monolayer agents, such as organosilanes[140], Tween 20 (REF.[142]) and cetyltrimethylammonium bromide[143], using covalent and non-covalent bonding strategies to functionalize the surface of silicon-nitride nanopores. A detailed description of several methods is provided in REF.[144]. Surface modifications not only improve molecular (DNA, RNA and proteins) transport kinetics but also mitigate irreversible adhesion. For example, a cationic organosilane, (3-aminopropyl)trimethoxysilane, was used[145] to increase the electrostatic interactions with DNA and transport speeds, especially at low pH. Moreover, dressing a pore with inorganic materials using ALD enables the fine-tuning of the surface properties (such as surface charge, roughness and chemical groups)[77,90,91]. Functionalization and pore-forming methods can also be used in combination, for example, using CDB[146].

An alternative functionalization strategy is to dress a fluid lipid bilayer around a nanopore to mimic biological structures, in which a curved membrane surface enhances sensing[147,148]. A biomimetic approach was developed[149] using lipid anchors as carriers of proteins and other molecules to the pore via membrane diffusion. Advantages of this method include a reduction of two orders of magnitude in translocation speeds, inhibited rotational dynamics and reduced non-specific adhesion of molecules to the pore surface. This method could be used to estimate the protein shape and dipole moment[150]. Lipid bilayers can be used to coat materials such as Al_2O_3 (REF.[151]), quartz[152,153] and graphene[154].

Finally, another strategy for pore functionalization is to attach a protein channel to a solid-state pore, combining the advantages of highly sensitive and reproducible biological nanopores with those of robust and non-diffusing solid-state nanopores. The first demonstration of hybrid nanopore formation[155] involved electrophoretically inserting α-haemolysin (α-HL) conjugated to a DNA tether into a 3.6 nm SiN pore, which could then be used to sense single-stranded DNA (ssDNA). Other hybrid pores comprising channels such as DNA origami[156] and viral portal proteins[157] were later demonstrated. In hybrid nanopore platforms, fluctuations in the signal are often observed, owing to leakage current caused by protein channel deformation and to the protein entering or exiting the solid-state pore. An ongoing research direction is to chemically bind the organic pore to the solid-state matrix with or without chemical conjugation[158–160], resulting in a fixed channel inserted in the solid-state pore with a well-defined position and orientation.

Surface modification for chemoselective detection. Nanopore sensing is an exceptionally versatile tool for the detection of biological analytes at the single-molecule level; however, it is generally not selective. Any molecule that can be electrokinetically driven through the nanopore can disrupt the flow of ions and produce a signal. The similarity in signal is particularly problematic in the discrimination of proteins, and solving this problem is essential for fingerprinting individual biomarkers and for screening complex biological fluids, such as serum, urine or cerebrospinal fluid. For example, human serum contains thousands of proteins in a broad range of concentrations, and the ability to detect a single protein type, especially at low concentrations, is critical for diagnostic and screening applications. There have been extensive efforts to address this limitation by incorporating a selective component to the detection modality. To date, nanopore selectivity has been achieved via two routes: functionalizing the nanopore with a receptor tailored for a specific analyte and introducing probes into the solution that can 'fish out' the molecules of interest (as will be discussed the next section).

Some of the earliest attempts to achieve selectivity have relied on chemical means to modify the nanopore surface, for both biological[161–163] and solid-state[164] nanopores. One common strategy was the use of DNA aptamers[22]. Aptamers are nucleic acids that bind to target molecules with high specificity and affinity. Unlike antibodies, aptamers[165,166] can be efficiently designed and selected to work in a range of buffer and pH conditions. One of the first instances was the attachment of a thrombin-binding aptamer to an α-HL pore. Thrombin, an enzyme with a crucial role in physiological and pathological coagulation, has been extensively used for the development of aptamer-based therapeutics and diagnostics, in large part because it is exceptionally well studied[167]. The DNA aptamer was covalently attached through a disulphide bond to a single cysteine residue near the opening of the pore. Upon binding to thrombin, the nanopore opening could be switched on and off by the cation-stabilized quadruplex formed by DNA, altering the ionic current. Although biological pores are not always as easy to modify as their solid-state analogues, they have the advantage that it is relatively easy to precisely control the site modification of the pore, along with the number of receptors that can be incorporated through site-directed mutagenesis[22,168,169], which enables the incorporation of different kinds of amino acids. By designing a mutant biological nanopore, more unique features can be added, such as the possibility of analysing characteristic frequency features inside the nanopore to map non-covalent interactions at the atomic scale[169].

Alternatively, in solid-state nanopores, functionality can be incorporated via the design of biomimetic platforms such as those incorporating single-protein receptors via a thiol-terminated self-assembled monolayer. Metallized silicon-nitride nanopores chemically modified with nitrilotriacetic-acid receptors allowed for the reversible binding and unbinding of proteins, which was observed in real time[170]. Although the functionalized site of the nanopore (the receptor) was arbitrarily located on the nanopore surface, it was possible to quantitatively determine the intrinsic binding strength (dissociation rate) of the molecular interactions from voltage-dependent measurements.

Selective sensing using molecular probes

Molecular carriers. The development of surface-functionalized pores has advanced a lot over the past decade. However, three further advances are needed: control over the receptor location for solid-state pores; ability to ensure that the target analyte (for example,

DNA or proteins) can produce a distinct signature and can be discriminated in complex biological fluids[17,18]; and the ability to detect rare analytes or analytes at very low concentration. The latter requirement arises from a fundamental limitation in conventional nanopore detection and is particularly challenging for small molecules and proteins, owing to their fast translocation times, close to or exceeding the bandwidth of modern current amplifiers, and to event rates often substantially lower than those predicted by the Smoluchowski equation, which is used to measure the rate of molecular capture at the entrance of a nanopore by free diffusion. This results in the need to use protein concentrations well over 10 nM (REF.[171]), a very high concentration when compared with that of many serum-based biomarkers.

Molecular carriers are particularly well suited to fulfil the above requirements. A carrier contains a selective (recognition) element that can be inserted into a solution (FIG. 2; TABLE 3). The translocation of a carrier with a bound analyte can be distinguished from that of the

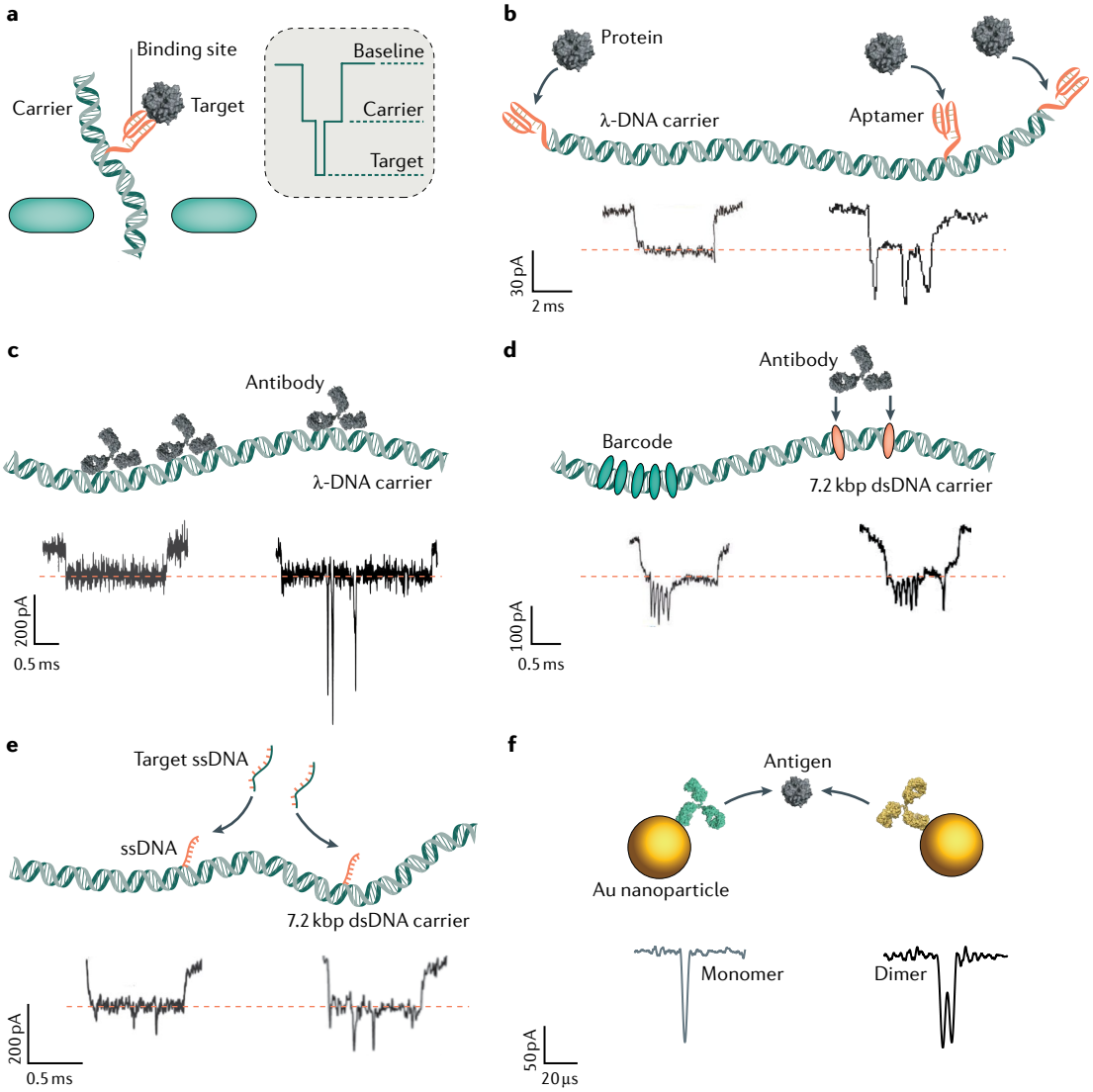

Fig. 2 | **Selective sensing of analytes using molecular carriers. a** | Schematic illustrating selective target detection using nanopore readout of molecular carriers. Bound targets are confirmed by the presence of one or multiple subpeaks, as shown in the inset. **b** | A λ-DNA carrier (48.5 kbp) engineered to incorporate three independent aptamer binding sites for multiplexed protein detection. **c** | A λ-DNA carrier used for the detection of arbitrarily bound anti-DNA antibodies. **d** | Digitally encoded 7.2 kbp double-stranded DNA (dsDNA) carrier used for multiplexed analysis of proteins. A 3-bit barcode was used to identify the different DNA carriers and respective targets. **e** | A 7.2 kbp dsDNA carrier used to bind and detect short, single-stranded DNA (ssDNA) sequences. The subtle structure difference between the unbound and bound states was identified using a high-bandwidth amplifier. **f** | Antigen detection based on nanoparticle dimerization. Two Au nanoparticle monomer probes with different antibodies self-assemble to form a dimer in the presence of the target antigen. The bound versus unbound state was identified based on the identification of a secondary single or double peak in the translocation signal[122]. Panel **b** adapted from REF.[18], CC BY 4.0. Panel **c** adapted with permission from REF.[24], American Chemical Society. Panel **d** adapted from REF.[172], Springer Nature Limited. Panel **e** adapted with permission from REF.[202], American Chemical Society. Panel **f**, R. Ren et al., unpublished work.

Table 3 | **Molecular carriers for selective analyte sensing**

Carrier type	Year	Nanopore	Molecular carrier	Functional group(s)	Target	Target concentration	Environment	Ref.
Biological Nanopores								
Polymer based	2011	α-HL	ssDNA	ATP-binding aptamer	ATP	μM	1 M KCl TE	208
	2013	α-HL	PNA + peptide	Complementary sequence	miRNA	pM–nM	0.5/3 M KCl	205
	2016	α-HL	PNA + peptide	Complementary sequence	10–90 nucleotides	nM	0.2/1 M KCl	207
	2016	α-HL	LNA-modified ssDNA	Complementary sequence	miRNA	nM	1 M KCl TE	206
	2018	α-HL	ssDNA	–	Cucurbituril	pM	3 M KCl TE	331
Solid-state Nanopores								
Nanoparticles	2012	Polyurethane (qNano)	25 nm NP	Complementary sequence	ssDNA	pM–nM	50 mM NaCl TE	189
	2013	Nanopipette (borosilicate/quartz)	10 nm NP	Peptide	Anti-peanut IgY antibody	–	15 mM PB	191
	2016	Polyurethane (qNano)	120 nm NP	Complementary sequence	Short ssDNA fragments	nM	PBS	187
	2017	Nanopipette (quartz)	5 nm NP	Lysozyme-binding aptamer	Lysozyme	pM–nM	100 mM KCl TE	26
	2018	Polyurethane (qNano)	120 nm NP	Complementary sequence and antibody	DNA methylation	–	PBS	332
	2019	Nanopipette (quartz)	11 nm NP	PNA	miRNA	nM	100 mM KCl PBS	188
Polymer based	2012	SiN	3 kbp DNA	–	γPNA	–	0.2/1 M KCl	333
	2014	SiN	dsDNA	Biotin	Monovalent streptavidin	nM–μM	900 mM NaCl and 6 mM PBS buffer	334
	2015	SiN	1 kbp dsDNA	Specific sequence	zif268/ zif268_GST	–	1 M KCl TE	196
	2015	SiN	5.6 kbp dsDNA	Specific sequence	Zinc finger protein	–	500 mM KCl TE	198
	2015	SiN	λ-DNA	–	Anti-DNA antibody	–	3 M KCl TE	24
	2015	Nanopipette (glass)	M13mp18 7.2 kbp DNA	Up to 3 biotin	Streptavidin	–	4 M LiCl TE	199
	2016	SiN	Biotinylated short ssDNA	Complementary sequence	miRNA	nM	900 mM NaCl 0.5 × PBS	335
	2016	Nanopipette (glass)	M13mp18 7.2 kbp DNA	Biotin/digoxigenin	Streptavidin/ anti-digoxigenin	nM	4 M LiCl TE	336
	2016	Nanopipette (glass)	7.2 kbp DNA with barcode	Biotin/BrdU/ puromycin/ digoxigenin	Anti-biotin/ BrdU/puromycin/ digoxigenin antibody	–	4 M LiCl TE	172
	2017	SiN	dsDNA scaffold	ATP-binding aptamer	ATP	–	3.6 M LiCl	337
	2017	Nanopipette (quartz)	λ-DNA	Thrombin/ AChE-binding aptamer	Thrombin/AChE	pM–nM	100 mM KCl TE + serum	18
	2017	Nanopipette (glass)	M13mp18 7.2 kbp DNA	Specific sequence	Single-nucleotide polymorphisms	–	4 M LiCl TE	338
	2017	SiN	ssDNA	PSA-binding aptamer	Prostate-specific antigen	nM	1 M KCl TE + serum	339
	2018	SiN	Biotinylated dsDNA	Biotin	Streptavidin	pM–nM	1 M KCl TE	314
	2018	Nanopipette (glass)	7.2 kbp DNA with barcode	ATP/thrombin/ lysozyme-binding aptamer	ATP/thrombin/ lysozyme	–	4 M LiCl TE	340

Table 3 (cont.) | **Molecular carriers for selective analyte sensing**

Carrier type	Year	Nanopore	Molecular carrier	Functional group(s)	Target	Target concentration	Environment	Ref.
Solid-state Nanopores (cont.)								
Polymer based (cont.)	2018	Nanopipette (quartz)	M13mp18 7.2 kbp DNA	Complementary sequence	Short ssDNA fragments	–	4 M LiCl TE	202
	2019	Nanopipette (quartz)	3.6 kbp dsDNA	Specific sequence	dCas9 protein	–	2–4 M LiCl TE	176
	2019	Nanopipette (quartz)	λ-DNA	Thrombin-binding aptamer	Thrombin	pM–nM	100 mM KCl TE + serum	17
	2019	SiN	M13mp18 7.2 kbp DNA	Complementary sequence	Tetrahedral DNA	–	1 M KCl TE	341
Origami	2018	SiN	DNA origami	Complementary sequence	Nucleoporins	–	250 mM KCl TE	204

AChE, acetylcholinesterase; ATP, adenosine triphosphate; BrdU, bromodeoxyuridine; dsDNA, double-stranded DNA; LNA, locked nucleic acid; miRNA, microRNA; NP, nanoparticle; PB, sodium phosphate buffer; PBS, phosphate-buffered saline; PNA, peptide nucleic acid; PSA, prostate-specific antigen; ssDNA, single-stranded DNA; TE, Tris-EDTA; α-HL, α-haemolysin; γPNA, γ-modified synthetic peptide nucleic acid.

carrier alone based on the ionic-current blockade, as the presence of the analyte induces a secondary peak superimposed on the signal[18,172,173]. The use of molecular carriers offers numerous advantages. First, the nanopore does not require any functional modifications. This keeps the platform generic in design, enabling the detection of different targets of interest and allowing the use of existing nanopore fabrication or synthesis methods. Second, analytes substantially smaller than the nanopore can be detected. This generally poses a challenge, as the signal-to-noise ratio is often governed by the excluded volume of the molecule[174]. The smaller the molecule relative to the pore size, the lower the signal-to-noise ratio. Third, molecular carriers such as DNA have a large and well-defined charge and are easily transported through a nanopore. Carriers enable more efficient transport and detection of analytes with a heterogeneous charge that may not otherwise translocate through the nanopore. An example is proteins that have a minimal charge or no net charge at all[175]. Fourth, the carriers can slow down transport through the nanopore, improving the signal-to-noise ratio. Fifth, multiplexing becomes possible by using different sites on the carriers to bind specific target analytes[18,172,176]. Of course, this comes with its own challenges, especially in cases when the carrier does not translocate through the nanopore at constant velocity. It is, therefore, essential to normalize the location of the subpeaks relative to the event duration to facilitate a comparison between different events[18,177]. Sixth, if the analyte has a low binding affinity, one can increase the carrier concentration to facilitate binding between the carrier and analyte. An often overlooked strategy general to all single-molecule methods is the use of a receptor to probe binding events well below the K_d (REF.[178]). For example, even if only a fraction of a per cent of a population is in the bound state, it is still possible to differentiate bound versus unbound events.

Functional nanoparticles. Functional nanoparticles are at the forefront of numerous sensing technologies, especially those incorporating optical methods such as absorption, fluorescence spectroscopy and Raman spectroscopy[179–181]. The popularity of nanoparticles is, in large part, due to their ease of functionalization with receptor ligands. For example, metallic nanoparticles can be functionalized using a single-step thiol[182,183] or amine[184,185] binding chemistry and oxide nanoparticles can also be functionalized using silanes[186].

Typical functionalization strategies produce a large number of binding sites on the nanoparticle, which efficiently concentrate analytes of interest, increasing the detected signal. In terms of nanopore sensing, such strategies have been used to detect targets such as oligonucleotides[187–190] or proteins[26,191,192]. Bare nanoparticles and nanoparticles with the bound target can be discriminated via a change in current, which also enables binding assays at ultra-low concentrations (FIG. 2f). For example[192], gold nanoparticles were decorated with an antibody selective to the cancer biomarker VEGF-C. Strategies combining functionalized surfaces and nanoparticles are also promising. In particular, a SiN pore was functionalized using silane chemistry with an anti-prostate-specific antigen, which was also bound to a magnetic nanoparticle decorated with another antibody that binds to prostate-specific antigen[178]. This platform can be used in whole blood and achieved an impressive detection limit of 0.8 fM.

To truly achieve single-molecule detection, it is essential to have one target per nanoparticle, otherwise, the unique information obtained from single molecules is lost. This is challenging owing to lack of control over the functionalization of nanoparticles with a well-defined number of receptors. A few strategies have been developed to solve this problem[193] but, to some extent, they still result in a distribution of targets on a single nanoparticle. DNA aptamer-modified gold nanoparticles with, on average, one nanoparticle per aptamer[26] were used to detect lysozyme with high selectivity and a dramatically improved capture rate as compared with the detection of bare proteins. More recently, a complementary strategy whereby nanoparticle dumbbells were formed upon binding to their respective targets (FIG. 2f) was shown to be even more selective and was used to perform single-molecule binding assays.

One advantage of using nanoparticles is that they can be easily concentrated using dielectrophoresis[194,195],

synthesized to manifest magnetic properties[188] and used to control the transport of bound analytes or increase their apparent concentration. However, the small size and spherical shape of nanoparticles lead to quick translocation, which is often very challenging to detect and demanding on state-of-the-art electronics. Moreover, the nanoparticle surface charge, combined with the electrolyte concentration, is often a source of spontaneous nanoparticle aggregation that has to be kept at bay by limiting the ionic strength of the buffer, often at the cost of a largely diminished detection signal.

DNA-based carriers. DNA-based carriers can be used to detect multiple bound analytes sequentially during translocation through a nanopore (FIG. 2b–e). Early examples include the detection of protein-bound ssDNA complexes[196,197] and the translocation of protein–double-stranded DNA (dsDNA) complexes and of anti-DNA antibodies bound to phage-λ DNA through a nanopore[24]. However, these molecules were randomly bound on the DNA-based carrier, in principle, upon confirmation of their presence in solution. More recently, precise control of the binding location has been achieved[198,199], which, in turn, improved detection throughput and minimized the false positives.

Several strategies have emerged to improve multiplexing and selectivity. For example, the detection of analytes bound to a molecular carrier based on M13mp18 7.2 kbp DNA was achieved using groups of small DNA hairpins functionalized with antibodies[172]. The specific binding sites along the backbone were read sequentially during translocation, allowing the detection of multiple fingerprint analytes with single-molecule resolution. A challenge is that both ends of the DNA carrier have the same probability of entering the pore, which complicates correlating the observed subpeaks to specific analytes. One solution is to encode DNA barcodes into the carrier, with each bit in the barcode signalled by the presence or absence of multiple DNA dumbbell hairpins. A 3-bit barcode could be assigned with 94% accuracy by electrophoretically driving the DNA through a solid-state nanopore[172] (FIG. 2d).

Molecular carriers also allow for the elucidation of protein structure and protein–protein interactions. For example, controlled unfolding and translocation of proteins through biological pores (α-HL) was demonstrated[200] using the AAA+ unfoldase ClpX. Sequence-dependent features of individual engineered proteins were detected during translocation, indicating that molecular motors can reproducibly drive proteins through a model nanopore, a feature required for protein sequencing using this single-molecule technology. Nanopore technology can also be used to recognize monoubiquitylated and polyubiquitylated forms of native proteins under physiological conditions[201].

Aside from using antibodies, the use of DNA probes coupled to carriers has also been explored. For example, high-bandwidth amplifiers were used along with nanopipettes to perform label-free detection of DNA sequences less than 100 nucleotides long[202] (FIG. 2e). An 88-mer target from the RV1910c gene in *Mycobacterium tuberculosis* could be detected when bound to its complementary strand. More recently, multiplexed DNA was detected specifically using dCas9-decorated dsDNA[176]. The target DNA, with one of two possible sequences, could be recognized by the presence of either double or triple peaks in the translocation signature when it was bound to the dCas9 probes. DNA aptamers have also shown great promise in screening a range of proteins in a multiplexed manner directly in biological fluids such as serum and urine. The combination of nanopore sensing and nucleic-acid aptamer recognition is highly advantageous, owing to the ease of multiplexing without the need for expensive labelling methods or sample pretreatment.

A unique advantage of DNA probes is that they are small and not easily detectable without the presence of a target molecule. In theory, the number of probes per molecular carrier is only limited by the spatial and temporal resolution of the nanopore and electronics. For example, it has been recently shown that 112 DNA hairpins can be detected and separated by 114 bp spacers, which opens up applications such as digital data storage, albeit at very high ionic strength[203]. It was also shown that two proteins with a ~96-bp spacing could be distinguished at physiological conditions[18].

Besides the use of single-stranded and double-stranded DNA carriers, advances in DNA nanotechnology have enabled the reliable synthesis of more complex DNA structures that can be used for biosensing. A DNA origami ring was fabricated[204] to contain eight binding sites that can recognize FG-nucleoporins (FG-Nups). The bare origami ring carrier, the carrier bound to FG-Nups and the carrier bound to mutated FG-Nups generated unique current-blockade signatures. Unlike carriers based on linear DNA, origami-based molecular carriers can be easily expanded to incorporate multiple binding sites.

In biological nanopores, the selective binding between the carrier and the target is reflected in long blockade signatures[205–207] due to the unzipping of the carrier–target complex and/or to conformational changes[208]. For example, a locked nucleic acid (LNA)-modified probe was fabricated to selectively sense specific microRNA (miRNA)[206]. When the LNA probe–miRNA duplex translocated through an α-HL nanopore, a unique two-level signal was observed. The conformational change of a G-quadruplex aptamer upon binding with adenosine triphosphate (ATP) could also be resolved by the translocation of aptamer and aptamer–ATP complexes through an α-HL nanopore[208]. This process can be seen as a two-level translocation event, indicating the binding of ATP with the aptamer. More recently, chemically modified single amino acids within a peptide were identified using a fragaceatoxin C nanopore[209]. The labelled and unlabelled protein could be clearly distinguished, showing the potential of the method for nanopore-based protein fingerprinting.

Sensor multiplexing. The time spent inside the detection volume ultimately governs how accurately a target–probe complex can be detected. A strategy first implemented by Marc Gershow and Jene Golovchenko was to read a translocating molecule over and over again

through a single pore by rapidly reversing the bias[210], reading the same molecule up to 12 times over 250 ms. This mode of detection was later complemented by the development of double-nanopore platforms for performing electrophoretic time-of-flight measurements[211] by determining the time it takes for a molecule to transit through two nanopores spaced 1.5 µm apart. More recently, there have been extensive efforts to reduce the spacing down to 10 nm to improve the capture and recapture efficiency[51,212,213]. With such small gaps, a molecule can be recaptured and even stalled with near 100% efficiency. This paves the way for targeted sensing with heightened sensitivity. Furthermore, the slower process facilitates recording translocations at lower bandwidth, improving the signal-to-noise ratio. It was shown that this strategy can be used not only to sense a single molecule of DNA by two nanopores but also to detect monovalent streptavidin bound to DNA using molecular carriers[213]. The method could be used to detect more biologically relevant molecules and could potentially even be used with fluids such as serum.

Alternative detection strategies

Nanopore FETs. Similar to nanopores, FET sensors can be used for label-free detection of biological species in solution or in complex biological media[2]. This has been demonstrated with Si nanowires[214], graphene[215] and carbon nanotubes[216]. The detection principle is based on monitoring the change in source–drain conductance or transient changes in gate conductance upon affinity-based binding of analytes on the transistor surface. Although promising, as for most sensors, a limitation is that analyte detection is diffusion-limited if the analyte is not actively transported to the FET. Furthermore, the active sensing volume is limited by the Debye screening length. Different approaches have been developed to address these issues, including working in dilute electrolytes, which effectively increases the Debye screening length, and functionalizing transistor channels with small receptors such as aptamers[217] and antibodies[218] to facilitate the detection of proteins[219] and viruses[220].

Integrating nanopores with FETs by confining charged analytes in a nanoscale pore offers several advantages, including the active transport of the analyte to the FET. Nanopore integration can be achieved using nanowires[32], graphene nanoribbons[33,34] and gold electrodes[28] aligned with the pore lumen (FIG. 3a–c). Detection in the FET and nanopore channel can be synchronized, as demonstrated for the detection of DNA[28,32–34] and nanoparticles[221]. The synchronization mechanism is based on either capacitive coupling[28,222], resulting from a change in local potential at the gate electrode during DNA translocation, or electrostatic gating[32,33,221,223] by the charge of the translocating molecule.

The concept of ionic FETs was first demonstrated by fabricating electrode-embedded nanopores by e-beam lithography and ALD[224]. The ionic transport in sub-10 nm nanopores could be effectively manipulated by using the electrodes embedded in the membrane. The control of analyte transport across the nanopores was also achieved for the single-molecule translocation of DNA[28,31,225,226]. More recently, double-barrelled nanopores have been used to control single-molecule transport via the integration of a gate electrode (FIG. 3d–f). The unique advantages of nanopores and FETs can be combined to obtain hybrid sensors with perfectly aligned nanopore and FET components able to detect molecular events with near 100% synchronization[28]. Surface functionalization of the gate electrode can fine-tune the transport properties, enabling the active control of the translocation velocity and capture rates. This approach can be used in combination with surface modifications with aptamers and antibodies to selectively target different proteins and even small molecules such as neurotransmitters, which are exceptionally challenging to detect using conventional nanopore platforms[225]. Although some improvements are still needed, the combination of nanopores and FETs has great potential to extract molecular fingerprints and possibly perform sequencing for a range of analytes[2,3,10].

Quantum tunnelling. A strategy to improve the spatial resolution in nanopores is based on quantum tunnelling. In a quantum-tunnelling configuration, two electrodes are placed close to each other, usually less than 5 nm apart, forming a junction for electrons to tunnel through. This detection method, in principle, can improve the spatial resolution with which the translocating analyte can be identified. Depending on the fabrication route, the electrodes can be suspended over the nanopore[227], embedded in a membrane[228] or layered between 2D insulators to form a tunnelling junction inside the nanopore[229,230] (FIG. 3g–i). The idea of combining nanopore detection and quantum tunnelling was, to some extent, inspired by the goal of achieving the future next-generation nucleic-acid sequencing[11,231]. This approach combines the advantages of nanopore single-molecule confinement and the high spatial, near-atomic resolution offered by tunnelling junctions, as initially demonstrated by STM. An early work from 2005 theoretically showed that quantum-tunnelling measurements can differentiate single nucleobases[232]. The study was followed by proposed designs for nanopore-based tunnelling architectures for nucleic-acid sequencing[233]. Around the same time, STM studies revealed that it is possible to measure the tunnelling current originating from nucleotide pairs and individual nucleic acids. These results fuelled the exploration of various designs based on nanopores with tunnelling or transverse electrodes[29,227,234–236].

Essential parameters that govern the measured tunnelling current are the distance and medium between the electrodes and the area of the tunnelling contact. A range of fabrication technologies, including mechanically controllable break junctions[237,238], electromigrated or burn junctions[239,240], advanced nanolithography[229], electron-beam-induced deposition[29,227] and feedback-controlled electrodeposition[241,242], have been optimized to build tunnelling sensors, usually employing gold and platinum for the electrodes. 2D materials, including graphene[232,243] and MoS_2 (REFS[232,244]), have also been proposed as electrode materials: their thickness, 3.35 Å and

6.5 Å, respectively, is very similar to that of individual nucleotides and amino acids.

Although initial work focused on nucleic acids, much effort has gone into the detection of proteins as a potential route towards protein sequencing and conformational analysis[245,246]. As the engineering of robust and stable junctions improves, quantum tunnelling might enable the identification with high sensitivity of particularly elusive essential biological molecules, such as polypeptides and small proteins[231]. However, as the tunnelling current exponentially depends on the size of the gap, fabricating small, stable junctions accurately aligned to the nanopore will be crucial. This will require extensive optimization to improve fabrication yield, suppress analyte absorption onto the surface of the tunnelling electrodes and improve analyte transport across the tunnelling junction and selectivity. A promising route to improved selectivity might be the incorporation of recognition chemistry to capture the analyte in the tunnelling junction[247,248].

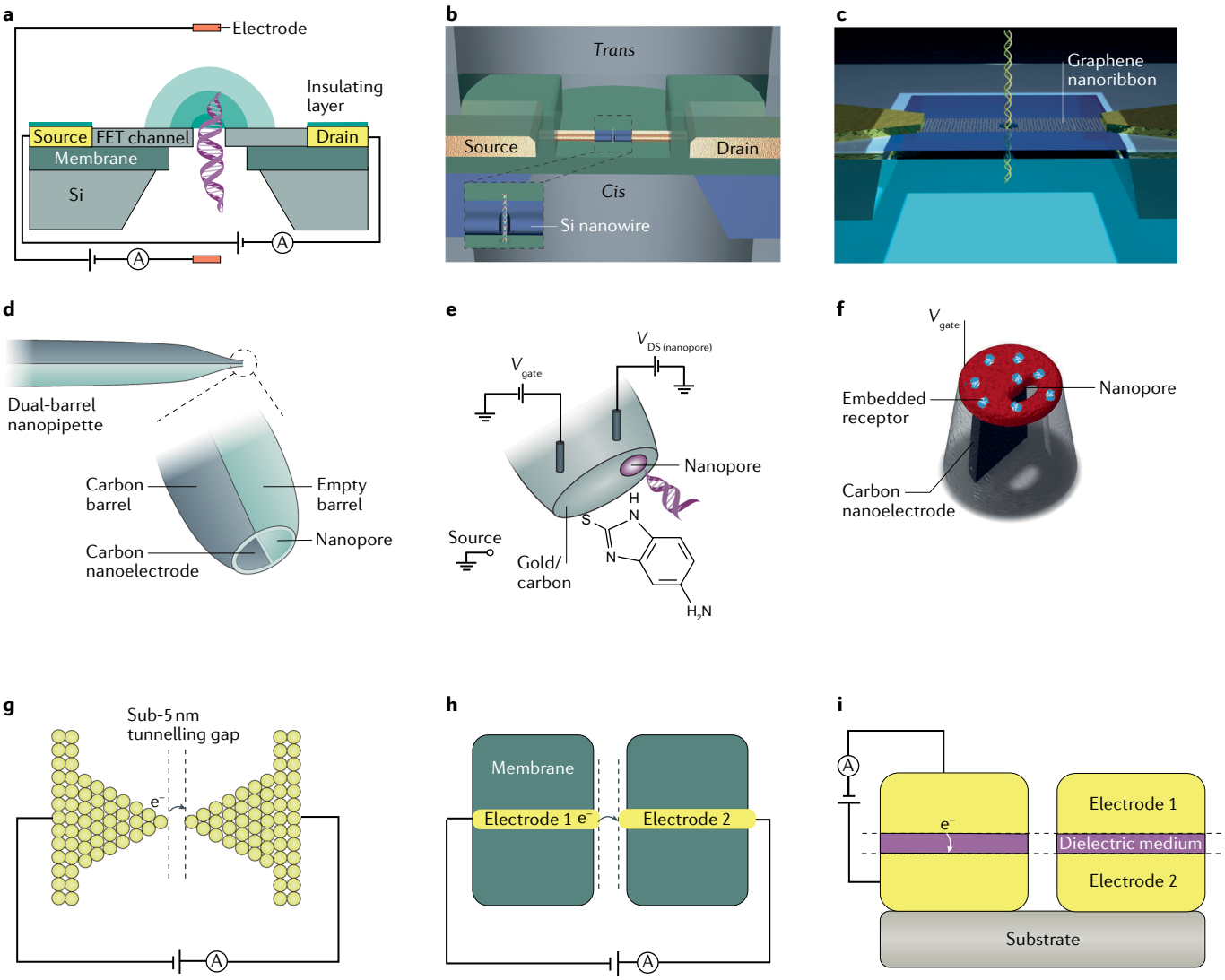

Fig. 3 | **Nanopore field-effect transistors and tunnelling junctions.** **a**–**c** | Solid-state nanopores can be integrated with field-effect transistors (FETs) by incorporating a drain–source channel aligned with the nanopore (panel **a**). Examples include Si nanowire nanopores (panel **b**) and graphene nanoribbon nanopores for the synchronized detection of single-molecule DNA translocation (panel **c**). **d** | Double-barrelled nanopore–FET devices can be fabricated from dual-barrel nanopipettes, with one barrel, filled with carbon via pyrolytic deposition from butane, forming a carbon nanoelectrode at the tip, and the other barrel, empty, used as the nanopore. **e** | Gold can then be electrochemically deposited on the carbon nanoelectrode and functionalized with thiolated species to be used as a gate to modulate single-molecule DNA translocation through the nanopore. **f** | The gate can be also fabricated by electropolymerization of pyrrole, and artificial receptors can be embedded within the polymeric film for selective single-molecule sensing of targeted analytes. **g**–**i** | Different approaches for fabricating tunnelling junctions. **g** | The tunnelling junction can be constituted by a pair of electrodes separated by a nanogap, formed via mechanically controllable breakdown, electron-beam-controlled deposition, electrochemical deposition or electroburning. **h** | Alternatively, tunnelling electrodes can be embedded in the membrane by advanced nanolithography techniques. **i** | Another approach consists of using a stacked architecture with a tunnelling medium possessing a high dielectric constant in the middle. With the constant advances in the semiconductor industry, the large-scale production of 3D stacked devices is possibly imminent. Panel **a** adapted with permission from REF.[343], American Chemical Society. Panel **b** adapted from REF.[32], Springer Nature Limited. Panel **c** adapted from REF.[34], Springer Nature Limited. Panel **e** adapted with permission from REF.[28], American Chemical Society. Panel **f** adapted from REF.[31], CC BY 4.0.

Photon-based sensing

Although sensing based on ionic currents provides an excellent time response and sensitivity, the throughput is often limited to a single nanopore. If multiple nanopores share the same electrodes, the signal-to-noise ratio decreases, the current signal from individual pores is convoluted and small molecules or small differences in molecules become difficult to discriminate. This limitation can be resolved if each nanopore is connected to an individual electrode and reservoir, but this is a challenging engineering task. However, other sensing methods can benefit from the molecular confinement offered by nanopores and provide extra information on top of the ionic current. Thus, there has been a drive to couple nanopore platforms with optical-sensing strategies, including the detection of single molecules labelled with a fluorescent dye with or without simultaneous electrical measurements; label-free molecule sensing based on fluorescent-ion indicators with multipore arrays; and plasmonic nanopores (FIG. 4). For details, we refer the reader to several reviews focusing specifically on photon-based sensing using nanopores[3,249–252].

Detection of fluorescently labelled molecules. Fluorescence spectroscopy is one of the most widely used methods for the detection of single molecules in solution. This is, in large part, due to the excellent signal that can be obtained from a single fluorophore. The underlying concept is that a fluorophore can be repeatedly cycled between its ground and excited states, as long as it is confined within the detection-probe volume and is not photobleached. For example, if a molecule has a fluorescence lifetime of 1 ns and resides in the probe volume for 1 ms, in theory, it can generate up to 1 million photons. In practice, this value is typically several orders of magnitude smaller owing to photobleaching, blinking, photodegradation and optical-collection efficiency (which is less than 0.2%)[253]. One of the key motivations for coupling single-molecule fluorescence with nanopores is to maximize the total number of photons recorded and reduce the background noise. Nanopores are exceptionally helpful in confining the analyte to a well-defined volume that is much smaller than a typical diffraction-limited probe volume. This substantially improves the overall photon-collection efficiency. Another advantage of using

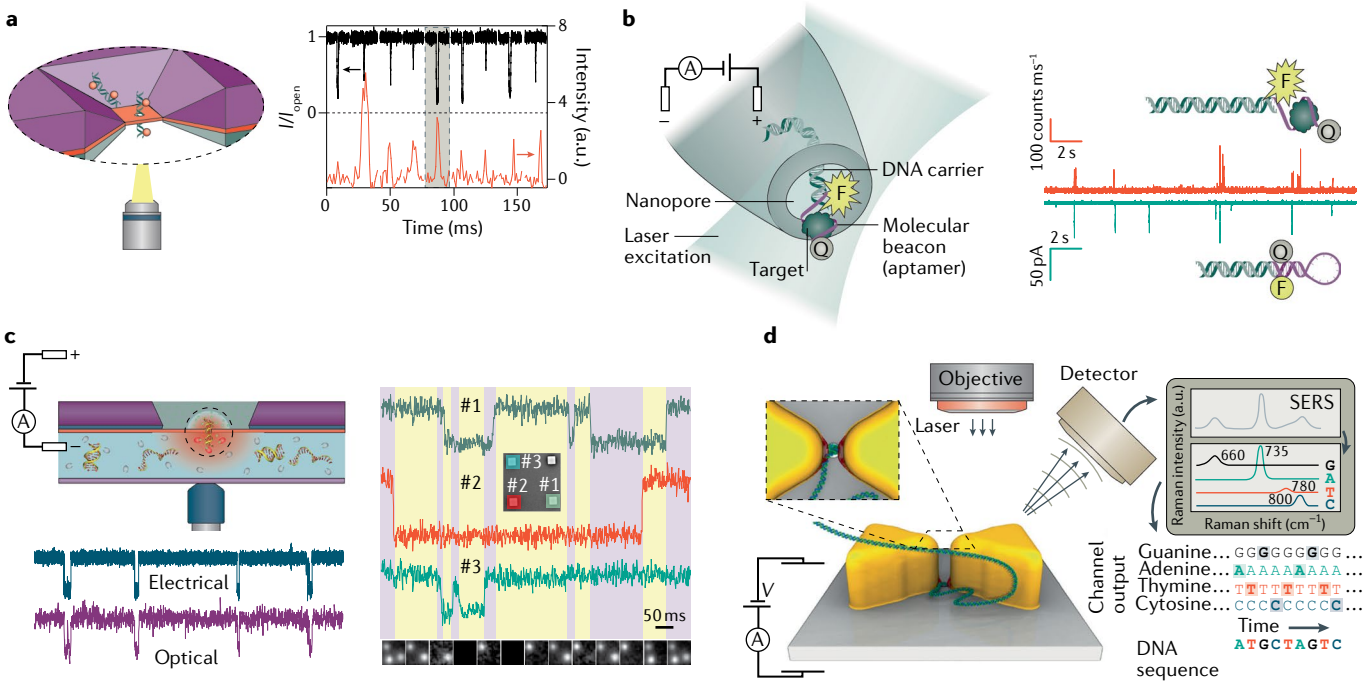

Fig. 4 | **Photon-based sensing. a** | Simultaneous fluorescence and ionic-current measurements. The schematic shows a typical optical-nanopore experiment. A fluorescent-dye-labelled DNA molecule (on the *cis* side) passes through a pore under an applied voltage, while an excitation laser is focused on the other side of the membrane (*trans* side). The optical (red) and electrical (black) traces recorded during the DNA translocation through the pore show synchronized fluorescence bursts and reductions of the electrical current. **b** | Selective sensing of proteins using DNA carriers coupled to molecular beacons encoded with an aptamer sequence. When there is no bound protein, only the ionic-current signal is observed (blue line), while when there is a protein bound to the DNA carrier, a signal in the optical channels is observed as well (red line), simultaneous to the electrical signal. **c** | Multipore measurement using fluorescent-ion indicators. Ca^{2+} ions are introduced in the *cis* chamber, whereas Ca^{2+} ion indicators are placed in the *trans* chamber. Under the applied voltage, Ca^{2+} ions passing through the nanopore bind with the indicators, leading to fluorescent emission with a signal-to-noise ratio comparable to that of the ion flux caused by single-molecule DNA translocation through the nanopore (left). This approach allows to simultaneously monitor the ion flux across several nanopores without compromising signal quality, as shown by the measurements on the right. The bottom images represent the consecutive fluorescence recordings of three independent nanopores. **d** | Plasmonic nanopores. A plasmonic bow-tie structure is fabricated next to a pore. When it is illuminated, a strong electromagnetic field is created locally, leading to enhanced optical signals (scattering light, fluorescence, Raman scattering, Förster resonance energy transfer) that can be used for DNA sequencing. SERS, surface-enhanced Raman spectroscopy. Panel **a** adapted from Soni et al. 2020 (REF.[267]), with the permission of AIP Publishing. Panel **b** adapted from REF.[17], CC BY 4.0. Panel **c** adapted with permission from REF.[274], American Chemical Society. Panel **d** adapted with permission from REF.[344], American Chemical Society.

solid-state nanopores is that complex multilayer structures can be designed not only to enhance fluorescence but also to minimize background noise.

Since the early 2000s, the passage of a dye-labelled DNA through a nanopore has been observed using both epifluorescence and confocal microscopy by merely tracking fluorescence bursts to probe diffusive and voltage-driven DNA dynamics near the pore[254–263]. In principle, single fluorophores can be observed, but in practice, detection is challenging. For example, DNA coil relaxation can be hindered in high-porosity membranes under ultraviolet laser illumination by electrokinetic force from the surrounding pores[264]. This enables the capture of molecules into laser-illuminated pores, in which maximum photon emission is expected. A DNA molecule translocating with a rate of ~10^4 nt ms^{-1} produces ~10^2 photons per passing nucleotide[35], but the strong fluorescence background from the membrane[265] and the autofluorescence from the buffer[266] make it difficult to identify single fluorescent dyes.

Several strategies have been developed to minimize losses, including the use of total internal reflection fluorescence microscopy, confocal microscopy and zero-mode waveguides (ZMWs). The synchronized optical and ionic currents generated by a dye-labelled DNA passing through a 4 nm pore was detected using total internal reflection fluorescence microscopy[267] (FIG. 4a). This method was further developed to detect DNA sequences using multicolour readout. In this strategy, a DNA template strand is recognized by molecular beacons with two types of fluorophore and translocates through a sub-2 nm pore. The nanopore sequentially unzips the beacons, leading to sequential fluorescence bursts that can be correlated to the template sequence[268]. ZMWs consist of small, metallic nanowells (typically made of aluminium) on a transparent substrate that reduces the background fluorescence, allowing for single-molecule detection and single-molecule real-time sequencing[269]. In the simplest design, an aluminium layer is deposited on top of a membrane, allowing dye-labelled single-DNA-translocation detection with high-contrast images[258,263]. Nanopores can be integrated into ZMWs to assist in single-molecule real-time sequencing, especially for long DNA molecules. Aluminium nanowells on a transparent membrane containing the pores were used to electrokinetically load single molecules, including DNA and DNA–protein complexes from low-concentration solutions (a few pM)[79,86,270].

Other ways to reduce the fluorescence of the background include thinning the SiN membrane to less than 5 nm (REF.[271]), replacing it with non-photoluminescent materials (such as SiO_2 or TiO_2)[81,91,270] and reducing the SiN photoluminescence by electron or ion-beam irradiation[265,272]. Recently, aptamer-based molecular beacons were introduced to identify single-nucleotide mismatches and target proteins directly in human serum and urine[17] (FIG. 4b). Often, these samples exhibit a substantial autofluorescent background; however, the nanopores can be used to suppress the background and increase the signal-to-noise ratio. However, because laser illumination of the nanopore produces electrical noise owing to fluctuating surface charges and the photoconductive effect, nanopore-chip design optimization is essential for obtaining high-bandwidth simultaneous optoelectrical measurement[95,273].

Molecular sensing with multipore arrays. In optical sensing, unlike in resistive-pulse sensing, the signal obtained from individual molecules does not decrease when the number of nanopores in the same membrane is increased. This allows the detection throughput to be increased by using optical detection in multipore arrays while retaining single-molecule resolution. One example is based on the detection of Ca^{2+} ion indicator dyes. Buffers containing Ca^{2+} are placed in the *cis* chamber and a Ca^{2+} indicator (such as Fluo-8 or Calbryte) in the *trans* chamber. Ca^{2+} diffusion through the pore generates a Ca^{2+} flux to the *trans* side, which results in ions binding to the dye and in a localized fluorescence signal (FIG. 4c). This method reveals the number and location of the pores, but also quantifies the ion flux at each pore[274,275]. It also enables the real-time visualization of nanopore formation by CDB[276,277], and was used to visualize pore localization with spatial resolution below the diffraction limit[277] and to monitor the flux of calcium ions through 24 pores on the same SiN membrane[278]. This approach is not restricted to Ca^{2+} ions, as indicators sensitive to other ions are available[279]. Droplet interface bilayers can also be used for sensing multipore arrays[280,281]. This platform can also be used to gain a fundamental understanding of membrane-protein diffusion in a lipid bilayer by tracking the position of the pore with time[282]. Recently, an electrode-free nanopore-measurement method, called DiffusiOptoPhysiology (DOP), was demonstrated. In this method, different salt species or different concentrations of the same salt are placed in the *cis* and *trans* chambers and produce unidirectional thermal diffusion of Ca^{2+} ions and an osmotic pressure that enables the detection of single molecules (for example, TriM-β-CD and dsDNA) without the application of an electrical potential[283].

Plasmonic nanopores. Plasmonic nanostructures produce a strong, localized electromagnetic field, the so-called plasmon resonance, and have attenuated background optical noise. Combined with nanopores, they, thus, promise optical detection with high signal-to-noise ratio during the recording of the ionic current (FIG. 4d). The modes of the plasmon resonance, which is the oscillation of a group of excited electrons that results in a strong electromagnetic field, depend on the geometry of the nanostructure, the wavelength of the excitation light and the surrounding medium.

Several plasmonic nanostructures have been integrated with nanopores, including bow-tie antennas[284], plasmonic nanowells[266], gold nanoparticles[56,285], plasmonic bullseye nanostructures[286,287] and plasmonic nanoslit cavities[134,288]. Because the plasmon resonance can enhance the light intensity by a factor of 10^4 (REF.[289]), single-molecule optical detection using scattering light[290–293], fluorescence[56,266], Raman scattering[294–298] and Förster resonance energy transfer[299] is achievable

in plasmonic nanopore systems. For example, the fluorescence from a single dye-labelled dsDNA was enhanced by a factor of 10 during its passage through a pore decorated with a plasmonic nanowell[266]. Localizing an electromagnetic field into sub-10 nm gold nanoslit structures loaded with ssDNA allowed the use of single-molecule, spatially resolved Raman spectroscopy[295]. If plasmonic structures are fabricated near the nanopore, as is the case for bow-tie antennas, scattering or transmitted light during the passage of DNA through the pore can be resolved, allowing label-free optoelectrical measurement with sub-millisecond temporal resolution[291–293].

In addition to sensing, plasmonic nanopores can be used for localized heating and molecular manipulation; indeed, laser illumination on a plasmonic pore results in photothermal heating of the pore surroundings[284,286,287,300]. This localized heating is accompanied by the formation of thermal gradients, resulting in phenomena such as molecular/ion thermophoresis[300–302] and localized bubble nucleation by heating of the solvent molecules[134]. Furthermore, the electromagnetic field generated at a plasmonic structure can efficiently trap single nanoparticles or proteins[303,304].

The combination of plasmonic nanoparticles and nanopores is an emerging field, and there are several reports on the integration of plasmonic structures with nanopores[56,285,305,306]. High-sensitivity molecular detection based on simultaneous optical and electrical readout using plasmonic nanopores will, no doubt, be the subject of exciting future research.

Machine-learning-assisted nanopore analysis

Single-molecule data contain much information, and recent advances in nanopore fabrication and detection mean we can access more of it. At the same time, there has been a steady improvement in our ability to record and classify single-molecule data and build more accurate models that allow us to recognize individual populations or specific features within a molecule. Recently, machine-learning algorithms have been gaining in prominence to assist in the analysis of data coming from nanopores. These algorithms are designed to pick up the most useful signatures, which are sometimes hidden, without explicit instruction and can be retrained using experimental datasets to further increase the detection accuracy.

One of the most sophisticated methods implemented to date is the use of deep neural networks for DNA sequencing. This approach facilitates the connection between the fingerprints of an enzymatic motor, the characteristic 'squiggle' signals from electrical recordings, sequence information and bioinformatics. Machine-learning approaches can be modified or customized for more applications, including the detection of DNA modifications[307], the discrimination of protein variants[308] and multiplexed detection of barcoded protein reporters[309]. Other algorithms such as convolutional neural networks[310], support vector machines[311,312] and time-series shapelets[313] were used to identify and analyse the parameters obtained from resistive-pulse sensing, resulting in increased accuracy and enhanced selectivity. Further applications include probing structural differences of tRNA[312], accurately detecting molecular-carrier barcoding[310], distinguishing mixed analytes of DNA oligomers with single-nucleotide differences[313] and quantifying glycosaminoglycans at the single-molecule level[311].

Conclusions

As nanopore-based DNA and RNA sequencing are achieving commercial success, we have provided a survey of alternative nanopore-based sensor configurations that employ novel materials and sensing modalities. The field of nanopores is ever-growing, with over a dozen companies pursuing the commercialization of nanopore-based sensing applications. This growth is a result of the realization that nanopores offer a unique combination of ultra-high-sensitivity detection with the possibility of identifying a molecule based on the signal generated by its transport through and interactions with the nanopore. Achieving specificity is perhaps the greatest challenge, as we have discussed. The incorporation of new modalities, such as combined optical and electronic detection, the use of chemical-recognition groups at the nanopore interface and machine-learning-based analysis are worth exploring further to enhance the spectrometric value of nanopore signals. On the detector end, combining electrical detection and fluorescence can provide a few-fold increase in specificity, and plasmonic devices can help localize light and enhance fluorescence signals. Ultimately, nanopores can assist with extracting photons from molecules to increase the signal-to-noise ratio. Furthermore, plasmonic devices allow for the use of alternative detection strategies such as Raman spectroscopy. Integrating tunnelling junctions into nanopores can help with multiplexing nanopore signals in an array format, as well as with providing tunnelling signals that are fingerprints of a particular type of molecule. The integration of FETs can aid with multiplexing to nanopore arrays, controlling analyte transport and improving detection at low-salt conditions. Although commercial strategies exist, further exploration of the possibility to scale up nanopore sensing is needed. This potentially has implications for the use of nanopores as diagnostic and screening tools. In addition to changes to the detector, alternative sample-preparation methods in which the analyte molecules are modified, such as by tagging them with various adapters or bulky groups, can greatly assist with increasing the specificity and sensitivity of nanopore sensors. Chemistry can also be used to enhance specificity by modifying the nanopore surface with functional groups that modulate interactions with the analyte. All of these sophistications require compatibility of the nanopore material with the method of interest, and many efforts have been devoted to identifying the most suitable materials for each detection method. It is certainly an exciting field to monitor as further progress is made with new nanopore materials, detection methods and molecular sensing applications.

Published online 21 September 2020

1. Feynman, R. P. in Engineering and Science Magazine Vol. XXIII 22–36 (California Institute of Technology, 1960).
2. Zhang, A. & Lieber, C. M. Nano-bioelectronics. *Chem. Rev.* **116**, 215–257 (2016).
3. Miles, B. N. et al. Single molecule sensing with solid-state nanopores: novel materials, methods, and applications. *Chem. Soc. Rev.* **42**, 15–28 (2013).
4. Sako, Y. & Yanagida, T. Single-molecule visualization in cell biology. *Nat. Rev. Mol. Cell Biol.* https://doi.org/10.1038/nrm1193 (2003).
5. Katan, A. J. & Dekker, C. High-speed AFM reveals the dynamics of single biomolecules at the nanometer scale. *Cell* **147**, 979–982 (2011).
6. Kodera, N., Yamamoto, D., Ishikawa, R. & Ando, T. Video imaging of walking myosin V by high-speed atomic force microscopy. *Nature* **468**, 72–76 (2010).
7. Zhang, B. et al. Role of contacts in long-range protein conductance. *Proc. Natl Acad. Sci. USA* **116**, 5886–5891 (2019).
8. Binnig, G. & Rohrer, H. Scanning tunneling microscopy. *Surf. Sci.* **126**, 236–244 (1983).
9. Hirschfeld, T. Optical microscopic observation of single small molecules. *J. Opt. Soc. Am.* **66**, 1124–1124 (1976).
10. Varongchayakul, N., Song, J., Meller, A. & Grinstaff, M. W. Single-molecule protein sensing in a nanopore: a tutorial. *Chem. Soc. Rev.* **47**, 8512–8524 (2018).
11. Lindsay, S. The promises and challenges of solid-state sequencing. *Nat. Nanotechnol.* **11**, 109–111 (2016).
12. Deamer, D., Akeson, M. & Branton, D. Three decades of nanopore sequencing. *Nat. Biotechnol.* **34**, 518–524 (2016).
13. Manrao, E. A. et al. Reading DNA at single-nucleotide resolution with a mutant MspA nanopore and phi29 DNA polymerase. *Nat. Biotechnol.* **30**, 349–353 (2012).
14. Rusk, N. MinION takes center stage. *Nat. Methods* **12**, 12–13 (2015).
15. Ashton, P. M. et al. MinION nanopore sequencing identifies the position and structure of a bacterial antibiotic resistance island. *Nat. Biotechnol.* **33**, 296–300 (2015).
16. Galenkamp, N. S., Soskine, M., Hermans, J., Wloka, C. & Maglia, G. Direct electrical quantification of glucose and asparagine from bodily fluids using nanopores. *Nat. Commun.* **9**, 4085 (2018).
17. Cai, S. L., Sze, J. Y. Y., Ivanov, A. P. & Edel, J. B. Small molecule electro-optical binding assay using nanopores. *Nat. Commun.* **10**, 1797 (2019).
18. Sze, J. Y. Y., Ivanov, A. P., Cass, A. E. G. & Edel, J. B. Single molecule multiplexed nanopore protein screening in human serum using aptamer modified DNA carriers. *Nat. Commun.* **8**, 1552 (2017).
19. Chinappi, M. & Cecconi, F. Protein sequencing via nanopore based devices: a nanofluidics perspective. *J. Phys. Condens. Matter.* **30**, 204002 (2018).
20. Restrepo-Perez, L., Joo, C. & Dekker, C. Paving the way to single-molecule protein sequencing. *Nat. Nanotechnol.* **13**, 786–796 (2018).
21. Yu, R. J., Ying, Y. L., Gao, R. & Long, Y. T. Confined nanopipette sensing: from single molecules, single nanoparticles, to single cells. *Angew. Chem. Int. Ed.* **58**, 3706–3714 (2019).
22. Rotem, D., Jayasinghe, L., Salichou, M. & Bayley, H. Protein detection by nanopores equipped with aptamers. *J. Am. Chem. Soc.* **134**, 2781–2787 (2012).
23. Qing, Y. J., Ionescu, S. A., Pulcu, G. S. & Bayley, H. Directional control of a processive molecular hopper. *Science* **361**, 908–911 (2018).
24. Plesa, C., Ruitenberg, J. W., Witteveen, M. J. & Dekker, C. Detection of individual proteins bound along DNA using solid-state nanopores. *Nano Lett.* **15**, 3153–3158 (2015).
25. Chien, C.-C., Shekar, S., Niedzwiecki, D. J., Shepard, K. L. & Drndić, M. Single-stranded DNA translocation recordings through solid-state nanopores on glass chips at 10 MHz measurement bandwidth. *ACS Nano* **13**, 10545–10554 (2019).
26. Lin, X. Y., Ivanov, A. P. & Edel, J. B. Selective single molecule nanopore sensing of proteins using DNA aptamer-functionalised gold nanoparticles. *Chem. Sci.* **8**, 3905–3912 (2017).
27. Cadinu, P., Kang, M., Nadappuram, B. P., Ivanov, A. P. & Edel, J. B. Individually addressable multi-nanopores for single-molecule targeted operations. *Nano Lett.* **20**, 2012–2019 (2020).
28. Xue, L. et al. Gated single-molecule transport in double-barreled nanopores. *ACS Appl. Mater. Interfaces* **10**, 38621–38629 (2018).
29. Ivanov, A. P. et al. DNA tunneling detector embedded in a nanopore. *Nano Lett.* **11**, 279–285 (2011).
30. Al Sulaiman, D., Cadinu, P., Ivanov, A. P., Edel, J. B. & Ladame, S. Chemically modified hydrogel-filled nanopores: a tunable platform for single-molecule sensing. *Nano Lett.* **18**, 6084–6093 (2018).
31. Ren, R. et al. Nanopore extended field-effect transistor for selective single-molecule biosensing. *Nat. Commun.* **8**, 586 (2017).
32. Xie, P., Xiong, Q., Fang, Y., Qing, Q. & Lieber, C. M. Local electrical potential detection of DNA by nanowire-nanopore sensors. *Nat. Nanotechnol.* **7**, 119–125 (2011).
33. Heerema, S. J. et al. Probing DNA translocations with inplane current signals in a graphene nanoribbon with a nanopore. *ACS Nano* **12**, 2623–2633 (2018).
34. Traversi, F. et al. Detecting the translocation of DNA through a nanopore using graphene nanoribbons. *Nat. Nanotechnol.* **8**, 939–945 (2013).
35. Venkatesan, B. M. & Bashir, R. Nanopore sensors for nucleic acid analysis. *Nat. Nanotechnol.* **6**, 615–624 (2011).
36. Li, J. et al. Ion-beam sculpting at nanometre length scales. *Nature* **412**, 166–169 (2001).
37. Storm, A. J., Chen, J. H., Ling, X. S., Zandbergen, H. W. & Dekker, C. Fabrication of solid-state nanopores with single-nanometre precision. *Nat. Mater.* **2**, 537–540 (2003).
38. Gierak, J. et al. Sub-5nm FIB direct patterning of nanodevices. *Microelectron. Eng.* **84**, 779–783 (2007).
39. Yang, J. et al. Rapid and precise scanning helium ion microscope milling of solid-state nanopores for biomolecule detection. *Nanotechnology* **22**, 285310 (2011).
40. Kennedy, E., Dong, Z., Tennant, C. & Timp, G. Reading the primary structure of a protein with 0.07 nm^3 resolution using a subnanometre-diameter pore. *Nat. Nanotechnol.* **11**, 968–976 (2016).
41. Rigo, E. et al. Measurements of the size and correlations between ions using an electrolytic point contact. *Nat. Commun.* **10**, 2382 (2019).
42. Kwok, H., Briggs, K. & Tabard-Cossa, V. Nanopore fabrication by controlled dielectric breakdown. *PLoS ONE* **9**, e92880 (2014).
43. Yanagi, I., Akahori, R., Hatano, T. & Takeda, K.-I. Fabricating nanopores with diameters of sub-1 nm to 3 nm using multilevel pulse-voltage injection. *Sci. Rep.* **4**, 5000 (2014).
44. Arcadia, C. E., Reyes, C. C. & Rosenstein, J. K. In situ nanopore fabrication and single-molecule sensing with microscale liquid contacts. *ACS Nano* **11**, 4907–4915 (2017).
45. Bandara, Y. M. N. D. Y., Karawdeniya, B. I. & Dwyer, J. R. Push-button method to create nanopores using a Tesla-Coil lighter. *ACS Omega* **4**, 226–230 (2019).
46. Zhang, Y. et al. Nanopore formation via tip-controlled local breakdown using an atomic force microscope. *Small Methods* **3**, 1900147 (2019).
47. Waugh, M. et al. Solid-state nanopore fabrication by automated controlled breakdown. *Nat. Protoc.* **15**, 122–143 (2020).
48. Wei, C., Bard, A. J. & Feldberg, S. W. Current rectification at quartz nanopipet electrodes. *Anal. Chem.* **69**, 4627–4633 (1997).
49. Piper, J. D., Clarke, R. W., Korchev, Y. E., Ying, L. & Klenerman, D. A renewable nanosensor based on a glass nanopipette. *J. Am. Chem. Soc.* **128**, 16462–16463 (2006).
50. Steinbock, L. J., Otto, O., Chimerel, C., Gornall, J. & Keyser, U. F. Detecting DNA folding with nanocapillaries. *Nano Lett.* **10**, 2493–2497 (2010).
51. Cadinu, P. et al. Double barrel nanopores as a new tool for controlling single-molecule transport. *Nano Lett.* **18**, 2738–2745 (2018).
52. Sun, L., Shigyou, K., Ando, T. & Watanabe, S. Thermally driven approach to fill sub-10-nm pipettes with batch production. *Anal. Chem.* **91**, 14080–14084 (2019).
53. Ayub, M. et al. Precise electrochemical fabrication of sub-20 nm solid-state nanopores for single-molecule biosensing. *J. Phys. Condens. Matter* **22**, 454128 (2010).
54. Rutkowska, A. et al. Electrodeposition and bipolar effects in metallized nanopores and their use in the detection of insulin. *Anal. Chem.* **87**, 2337–2344 (2015).
55. Choi, J., Lee, C. C. & Park, S. Scalable fabrication of sub-10 nm polymer nanopores for DNA analysis. *Microsyst. Nanoeng.* **5**, 12 (2019).
56. Nam, S. et al. Graphene nanopore with a self-integrated optical antenna. *Nano Lett.* **14**, 5584–5589 (2014).
57. de Vreede, L. J., van den Berg, A. & Eijkel, J. C. T. Nanopore fabrication by heating Au particles on ceramic substrates. *Nano Lett.* **15**, 727–731 (2015).
58. de Vreede, L. J., Muniz, M. S., van den Berg, A. & Eijkel, J. C. T. Nanopore fabrication in silicon oxynitride membranes by heating Au-particles. *J. Micromech. Microeng.* **26**, 037001 (2016).
59. Apel, P. Y., Korchev, Y. E., Siwy, Z., Spohr, R. & Yoshida, M. Diode-like single-ion track membrane prepared by electro-stopping. *Nucl. Instrum. Methods. Phys. Res. B* **184**, 337–346 (2001).
60. Siwy, Z. S. et al. Calcium-induced voltage gating in single conical nanopores. *Nano Lett.* **6**, 1729–1734 (2006).
61. Vlassiouk, I., Apel, P. Y., Dmitriev, S. N., Healy, K. & Siwy, Z. S. Versatile ultrathin nanoporous silicon nitride membranes. *Proc. Natl Acad. Sci. USA* **106**, 21039–21044 (2009).
62. Park, S. R., Peng, H. & Ling, X. S. Fabrication of nanopores in silicon chips using feedback chemical etching. *Small* **3**, 116–119 (2007).
63. Schmidt, T., Zhang, M., Sychugov, I., Roxhed, N. & Linnros, J. Nanopore arrays in a silicon membrane for parallel single-molecule detection: fabrication. *Nanotechnology* **26**, 314001 (2015).
64. Chen, Q., Wang, Y., Deng, T. & Liu, Z. Fabrication of nanopores and nanoslits with feature sizes down to 5 nm by wet etching method. *Nanotechnology* **29**, 085301 (2018).
65. Tsujino, K. & Matsumura, M. Boring deep cylindrical nanoholes in silicon using silver nanoparticles as a catalyst. *Adv. Mater.* **17**, 1045–1047 (2005).
66. James, T. et al. Voltage-gated ion transport through semiconducting conical nanopores formed by metal nanoparticle-assisted plasma etching. *Nano Lett.* **12**, 3437–3442 (2012).
67. Lee, K. et al. Recent progress in solid-state nanopores. *Adv. Mater.* **30**, 1704680 (2018).
68. Chen, Q. & Liu, Z. Fabrication and applications of solid-state nanopores. *Sensors* **19**, 1886 (2019).
69. Danda, G. & Drndić, M. Two-dimensional nanopores and nanoporous membranes for ion and molecule transport. *Curr. Opin. Biotechnol.* **55**, 124–133 (2019).
70. Wu, M.-Y., Krapf, D., Zandbergen, M., Zandbergen, H. & Batson, P. E. Formation of nanopores in a SiN/SiO_2 membrane with an electron beam. *Appl. Phys. Lett.* **87**, 113106 (2005).
71. Kim, M. J., Wanunu, M., Bell, D. C. & Meller, A. Rapid fabrication of uniformly sized nanopores and nanopore arrays for parallel DNA analysis. *Adv. Mater.* **18**, 3149–3153 (2006).
72. van den Hout, M. et al. Controlling nanopore size, shape and stability. *Nanotechnology* **21**, 115304 (2010).
73. Wanunu, M. et al. Rapid electronic detection of probe-specific microRNAs using thin nanopore sensors. *Nat. Nanotechnol.* **5**, 807–814 (2010).
74. Sawafta, F., Carlsen, A. T. & Hall, A. R. Membrane thickness dependence of nanopore formation with a focused helium ion beam. *Sensors* **14**, 8150–8161 (2014).
75. Rodríguez-Manzo, J. A., Puster, M., Nicolaï, A., Meunier, V. & Drndić, M. DNA translocation in nanometer thick silicon nanopores. *ACS Nano* **9**, 6555–6564 (2015).
76. Gilboa, T., Zrehen, A., Girsault, A. & Meller, A. Optically-monitored nanopore fabrication using a focused laser beam. *Sci. Rep.* **8**, 9765 (2018).
77. Yamazaki, H., Hu, R., Zhao, Q. & Wanunu, M. Photothermally assisted thinning of silicon nitride membranes for ultrathin asymmetric nanopores. *ACS Nano* **12**, 12472–12481 (2018).
78. Yanagi, I., Hamamura, H., Akahori, R. & Takeda, K.-I. Two-step breakdown of a SiN membrane for nanopore fabrication: Formation of thin portion and penetration. *Sci. Rep.* **8**, 10129 (2018).
79. Larkin, J., Henley, R. Y., Jadhav, V., Korlach, J. & Wanunu, M. Length-independent DNA packing into nanopore zero-mode waveguides for low-input DNA sequencing. *Nat. Nanotechnol.* **12**, 1169–1175 (2017).
80. Merchant, C. A. et al. DNA translocation through graphene nanopores. *Nano Lett.* **10**, 2915–2921 (2010).
81. Wang, R. et al. Single-molecule discrimination of labeled DNAs and polypeptides using photoluminescent-free TiO_2 nanopores. *ACS Nano* **12**, 11648–11656 (2018).

82. Sainiemi, L., Grigoras, K. & Franssila, S. Suspended nanostructured alumina membranes. *Nanotechnology* **20**, 075306 (2009).
83. Venkatesan, B. M. et al. Highly sensitive, mechanically stable nanopore sensors for DNA analysis. *Adv. Mater.* **21**, 2771–2776 (2009).
84. Venkatesan, B. M., Shah, A. B., Zuo, J.-M. & Bashir, R. DNA sensing using nanocrystalline surface-enhanced Al_2O_3 nanopore sensors. *Adv. Funct. Mater.* **20**, 1266–1275 (2010).
85. Wang, L. et al. Ultrathin oxide films by atomic layer deposition on graphene. *Nano Lett.* **12**, 3706–3710 (2012).
86. Jadhav, V., Hoogerheide, D. P., Korlach, J. & Wanunu, M. Porous zero-mode waveguides for picogram-level DNA capture. *Nano Lett.* **19**, 921–929 (2019).
87. Venkatesan, B. M. et al. Stacked graphene-Al_2O_3 nanopore sensors for sensitive detection of DNA and DNA–protein complexes. *ACS Nano* **6**, 441–450 (2012).
88. Larkin, J. et al. Slow DNA transport through nanopores in hafnium oxide membranes. *ACS Nano* **7**, 10121–10128 (2013).
89. Shim, J., Rivera, J. A. & Bashir, R. Electron beam induced local crystallization of HfO_2 nanopores for biosensing applications. *Nanoscale* **5**, 10887–10893 (2013).
90. Chen, P. et al. Atomic layer deposition to fine-tune the surface properties and diameters of fabricated nanopores. *Nano Lett.* **4**, 1333–1337 (2004).
91. dela Torre, R., Larkin, J., Singer, A. & Meller, A. Fabrication and characterization of solid-state nanopore arrays for high-throughput DNA sequencing. *Nanotechnology* **23**, 385308 (2012).
92. Cabello-Aguilar, S. et al. Slow translocation of polynucleotides and their discrimination by α-hemolysin inside a single track-etched nanopore designed by atomic layer deposition. *Nanoscale* **5**, 9582–9586 (2013).
93. Sze, J. Y. Y., Kumar, S., Ivanov, A. P., Oh, S. H. & Edel, J. B. Fine tuning of nanopipettes using atomic layer deposition for single molecule sensing. *Analyst* **140**, 4828–4834 (2015).
94. Park, K.-B. et al. Highly reliable and low-noise solid-state nanopores with an atomic layer deposited ZnO membrane on a quartz substrate. *Nanoscale* **9**, 18772–18780 (2017).
95. Pitchford, W. H. et al. Synchronized optical and electronic detection of biomolecules using a low noise nanopore platform. *ACS Nano* **9**, 1740–1748 (2015).
96. Wang, Y., Chen, Q., Deng, T. & Liu, Z. Nanopore fabricated in pyramidal HfO_2 film by dielectric breakdown method. *Appl. Phys. Lett.* **111**, 143103 (2017).
97. Wang, Y., Chen, Q., Deng, T. & Liu, Z. Self-aligned nanopore formed on a SiO_2 pyramidal membrane by a multipulse dielectric breakdown method. *J. Phys. Chem. C* **122**, 11516–11523 (2018).
98. Garaj, S. et al. Graphene as a subnanometre trans-electrode membrane. *Nature* **467**, 190–193 (2010).
99. Schneider, G. F. et al. DNA translocation through graphene nanopores. *Nano Lett.* **10**, 3163–3167 (2010).
100. Waduge, P., Larkin, J., Upmanyu, M., Kar, S. & Wanunu, M. Programmed synthesis of freestanding graphene nanomembrane arrays. *Small* **11**, 597–603 (2015).
101. Walker, M. I., Weatherup, R. S., Bell, N. A. W., Hofmann, S. & Keyser, U. F. Free-standing graphene membranes on glass nanopores for ionic current measurements. *Appl. Phys. Lett.* **106**, 023119 (2015).
102. Schneider, G. F. et al. Tailoring the hydrophobicity of graphene for its use as nanopores for DNA translocation. *Nat. Commun.* **4**, 2619 (2013).
103. Balan, A., Chien, C.-C., Engelke, R. & Drndić, M. Suspended solid-state membranes on glass chips with sub 1-pF capacitance for biomolecule sensing applications. *Sci. Rep.* **5**, 17775 (2015).
104. Liu, S. et al. Boron nitride nanopores: highly sensitive DNA single-molecule detectors. *Adv. Mater.* **25**, 4549–4554 (2013).
105. Zhou, Z. et al. DNA translocation through hydrophilic nanopore in hexagonal boron nitride. *Sci. Rep.* **3**, 3287 (2013).
106. Park, K.-B. et al. Noise and sensitivity characteristics of solid-state nanopores with a boron nitride 2-D membrane on a pyrex substrate. *Nanoscale* **8**, 5755–5763 (2016).
107. Liu, K., Feng, J., Kis, A. & Radenovic, A. Atomically thin molybdenum disulfide nanopores with high sensitivity for DNA translocation. *ACS Nano* **8**, 2504–2511 (2014).
108. Waduge, P. et al. Direct and scalable deposition of atomically thin low-noise MoS_2 membranes on apertures. *ACS Nano* **9**, 7352–7359 (2015).
109. Danda, G. et al. Monolayer WS_2 nanopores for DNA translocation with light-adjustable sizes. *ACS Nano* **11**, 1937–1945 (2017).
110. Shen, Y. et al. In situ repair of 2D chalcogenides under electron beam irradiation. *Adv. Mater.* **30**, 1705954 (2018).
111. Mojtabavi, M., VahidMohammadi, A., Liang, W., Beidaghi, M. & Wanunu, M. Single-molecule sensing using nanopores in two-dimensional transition metal carbide (MXene) membranes. *ACS Nano* **13**, 3042–3053 (2019).
112. Cun, H. et al. Wafer-scale MOCVD growth of monolayer MoS_2 on sapphire and SiO_2. *Nano Res.* **12**, 2646–2652 (2019).
113. Graf, M. et al. Fabrication and practical applications of molybdenum disulfide nanopores. *Nat. Protoc.* **14**, 1130–1168 (2019).
114. Song, B. et al. Atomic-scale electron-beam sculpting of near-defect-free graphene nanostructures. *Nano Lett.* **11**, 2247–2250 (2011).
115. Emmrich, D. et al. Nanopore fabrication and characterization by helium ion microscopy. *Appl. Phys. Lett.* **108**, 163103 (2016).
116. Gilbert, S. M., Liu, S., Schumm, G. & Zettl, A. Nanopatterning hexagonal boron nitride with helium ion milling: towards atomically-thin, nanostructured insulators. *MRS Adv.* **3**, 327–331 (2018).
117. Kuan, A. T., Lu, B., Xie, P., Szalay, T. & Golovchenko, J. A. Electrical pulse fabrication of graphene nanopores in electrolyte solution. *Appl. Phys. Lett.* **106**, 203109 (2015).
118. Feng, J. et al. Electrochemical reaction in single layer MoS_2: nanopores opened atom by atom. *Nano Lett.* **15**, 3431–3438 (2015).
119. Surwade, S. P. et al. Water desalination using nanoporous single-layer graphene. *Nat. Nanotechnol.* **10**, 459–464 (2015).
120. Feng, J. et al. Identification of single nucleotides in MoS2 nanopores. *Nat. Nanotechnol.* **10**, 1070–1076 (2015).
121. Liang, S. et al. Noise in nanopore sensors: sources, models, reduction, and benchmarking. *Nanotechnol. Precis. Eng.* **3**, 9–17 (2020).
122. Fragasso, A., Schmid, S. & Dekker, C. Comparing current noise in biological and solid-state nanopores. *ACS Nano* **14**, 1338–1349 (2020).
123. Uram, J. D., Ke, K. & Mayer, M. Noise and bandwidth of current recordings from submicrometer pores and nanopores. *ACS Nano* **2**, 857–872 (2008).
124. Rosenstein, J. K., Wanunu, M., Merchant, C. A., Drndic, M. & Shepard, K. L. Integrated nanopore sensing platform with sub-microsecond temporal resolution. *Nat. Methods* **9**, 487–492 (2012).
125. Tabard-Cossa, V., Trivedi, D., Wiggin, M., Jetha, N. N. & Marziali, A. Noise analysis and reduction in solid-state nanopores. *Nanotechnology* **18**, 305505 (2007).
126. Lee, M.-H. et al. A low-noise solid-state nanopore platform based on a highly insulating substrate. *Sci. Rep.* **4**, 7448 (2014).
127. de Vreede, L. et al. Wafer scale fabrication of fused silica chips for low-noise recording of resistive pulses through nanopores. *Nanotechnology* **30**, 265301 (2019).
128. Choi, W. et al. A low-noise silicon nitride nanopore device on a polymer substrate. *PLoS ONE* **13**, e0200831 (2018).
129. Xia, P. et al. Sapphire nanopores for low-noise DNA sensing. Preprint at *bioRxiv* 2020.03.02.973826 (2020).
130. Fragasso, A., Pud, S. & Dekker, C. 1/*f* noise in solid-state nanopores is governed by access and surface regions. *Nanotechnology* **30**, 395202 (2019).
131. Radenovic, A., Trepagnier, E., Csencsits, R., Downing, K. H. & Liphardt, J. Fabrication of 10 nm diameter hydrocarbon nanopores. *Appl. Phys. Lett.* **93**, 183101 (2008).
132. Hoogerheide, D. P., Garaj, S. & Golovchenko, J. A. Probing surface charge fluctuations with solid-state nanopores. *Phys. Rev. Lett.* **102**, 256804 2009).
133. Smeets, R. M. M., Keyser, U. F., Wu, M. Y., Dekker, N. H. & Dekker, C. Nanobubbles in solid-state nanopores. *Phys. Rev. Lett.* **97**, 088101 (2006).
134. Li, Y. et al. Photoresistance switching of plasmonic nanopores. *Nano Lett.* **15**, 776–782 (2015).
135. Gravelle, S., Netz, R. R. & Bocquet, L. Adsorption kinetics in open nanopores as a source of low-frequency noise. *Nano Lett.* **19**, 7265–7272 (2019).
136. Beamish, E., Kwok, H., Tabard-Cossa, V. & Godin, M. Precise control of the size and noise of solid-state nanopores using high electric fields. *Nanotechnology* **23**, 405301 (2012).
137. Kumar, A., Park, K.-B., Kim, H.-M. & Kim, K.-B. Noise and its reduction in graphene based nanopore devices. *Nanotechnology* **24**, 495503 (2013).
138. Heerema, S. J. et al. 1/f noise in graphene nanopores. *Nanotechnology* **26**, 074001 (2015).
139. Wen, C. et al. Generalized noise study of solid-state nanopores at low frequencies. *ACS Sens.* **2**, 300–307 (2017).
140. Wanunu, M. & Meller, A. Chemically modified solid-state nanopores. *Nano Lett.* **7**, 1580–1585 (2007).
141. Wei, R., Pedone, D., Zürner, A., Döblinger, M. & Rant, U. Fabrication of metallized nanopores in silicon nitride membranes for single-molecule sensing. *Small* **6**, 1406–1414 (2010).
142. Hu, R. et al. Intrinsic and membrane-facilitated α-synuclein oligomerization revealed by label-free detection through solid-state nanopores. *Sci. Rep.* **6**, 20776 (2016).
143. Xie, Y. et al. Surface modification of single track-etched nanopores with surfactant CTAB. *Langmuir* **25**, 8870–8874 (2009).
144. Eggenberger, O. M., Ying, C. & Mayer, M. Surface coatings for solid-state nanopores. *Nanoscale* **11**, 19636–19657 (2019).
145. Anderson, B. N., Muthukumar, M. & Meller, A. pH tuning of DNA translocation time through organically functionalized nanopores. *ACS Nano* **7**, 1408–1414 (2013).
146. Bandara, Y. M. N. D. Y., Karawdeniya, B. I., Hagan, J. T., Chevalier, R. B. & Dwyer, J. R. Chemically functionalizing controlled dielectric breakdown silicon nitride nanopores by direct photohydrosilylation. *ACS Appl. Mater. Interfaces* **11**, 30411–30420 (2019).
147. Ying, C. et al. Formation of single nanopores with diameters of 20–50 nm in silicon nitride membranes using laser-assisted controlled breakdown. *ACS Nano* **12**, 11458–11470 (2018).
148. Yusko, E. C. et al. Controlling protein translocation through nanopores with bio-inspired fluid walls. *Nat. Nanotechnol.* **6**, 253–260 (2011).
149. Yusko, E. C. et al. Real-time shape approximation and fingerprinting of single proteins using a nanopore. *Nat. Nanotechnol.* **12**, 360–367 (2016).
150. Houghtaling, J. et al. Estimation of shape, volume, and dipole moment of individual proteins freely transiting a synthetic nanopore. *ACS Nano* **13**, 5231–5242 (2019).
151. Venkatesan, B. M. et al. Lipid bilayer coated Al_2O_3 nanopore sensors: towards a hybrid biological solid-state nanopore. *Biomed. Microdevices* **13**, 671–682 (2011).
152. Hernández-Ainsa, S. et al. Lipid-coated nanocapillaries for DNA sensing. *Analyst* **138**, 104–106 (2013).
153. Gutsmann, T., Heimburg, T., Keyser, U., Mahendran, K. R. & Winterhalter, M. Protein reconstitution into freestanding planar lipid membranes for electrophysiological characterization. *Nat. Protoc.* **10**, 188–198 (2015).
154. Shan, Y. P. et al. Surface modification of graphene nanopores for protein translocation. *Nanotechnology* **24**, 495102–495102 (2013).
155. Hall, A. R. et al. Hybrid pore formation by directed insertion of α-haemolysin into solid-state nanopores. *Nat. Nanotechnol.* **5**, 874–877 (2010).
156. Bell, N. A. W. et al. DNA origami nanopores. *Nano Lett.* **12**, 512–517 (2012).
157. Cressiot, B., Greive, S. J., Mojtabavi, M., Antson, A. A. & Wanunu, M. Thermostable virus portal proteins as reprogrammable adapters for solid-state nanopore sensors. *Nat. Commun.* **9**, 4652 (2018).
158. Langecker, M. et al. Synthetic lipid membrane channels formed by designed DNA nanostructures. *Science* **338**, 932–936 (2012).
159. Burns, J. R., Stulz, E. & Howorka, S. Self-assembled DNA nanopores that span lipid bilayers. *Nano Lett.* **13**, 2351–2356 (2013).
160. Cressiot, B. et al. Porphyrin-assisted docking of a thermophage portal protein into lipid bilayers: nanopore engineering and characterization. *ACS Nano* **11**, 11931–11945 (2017).
161. Fahie, M., Chisholm, C. & Chen, M. Resolved single-molecule detection of individual species within a mixture of anti-biotin antibodies using an engineered monomeric nanopore. *ACS Nano* **9**, 1089–1098 (2015).
162. Wu, H. C. & Bayley, H. Single-molecule detection of nitrogen mustards by covalent reaction within a protein nanopore. *J. Am. Chem. Soc.* **130**, 6813–6819 (2008).

163. Clarke, J. et al. Continuous base identification for single-molecule nanopore DNA sequencing. *Nat. Nanotechnol.* **4**, 265–270 (2009).
164. Wang, G. L., Zhang, B., Wayment, J. R., Harris, J. M. & White, H. S. Electrostatic-gated transport in chemically modified glass nanopore electrodes. *J. Am. Chem. Soc.* **128**, 7679–7686 (2006).
165. Fang, X. H. & Tan, W. H. Aptamers generated from cell-SELEX for molecular medicine: a chemical biology approach. *Acc. Chem. Res.* **43**, 48–57 (2010).
166. Wilson, D. S. & Szostak, J. W. In vitro selection of functional nucleic acids. *Annu. Rev. Biochem.* **68**, 611–647 (1999).
167. Bock, L. C., Griffin, L. C., Latham, J. A., Vermaas, E. H. & Toole, J. J. Selection of single-stranded-DNA molecules that bind and inhibit human thrombin. *Nature* **355**, 564–566 (1992).
168. Soskine, M. et al. An engineered ClyA nanopore detects folded target proteins by selective external association and pore entry. *Nano Lett.* **12**, 4895–4900 (2012).
169. Ying, Y.-L. & Long, Y.-T. Nanopore-based single-biomolecule interfaces: from information to knowledge. *J. Am. Chem. Soc.* **141**, 15720–15729 (2019).
170. Wei, R. S., Gatterdam, V., Wieneke, R., Tampe, R. & Rant, U. Stochastic sensing of proteins with receptor-modified solid-state nanopores. *Nat. Nanotechnol.* **7**, 257–263 (2012).
171. Plesa, C. et al. Fast translocation of proteins through solid state nanopores. *Nano Lett.* **13**, 658–663 (2013).
172. Bell, N. A. W. & Keyser, U. F. Digitally encoded DNA nanostructures for multiplexed, single-molecule protein sensing with nanopores. *Nat. Nanotechnol.* **11**, 645–651 (2016).
173. Yang, W. et al. Detection of CRISPR-dCas9 on DNA with solid-state nanopores. *Nano Lett.* **18**, 6469–6474 (2018).
174. Talaga, D. S. & Li, J. L. Single-molecule protein unfolding in solid state nanopores. *J. Am. Chem. Soc.* **131**, 9287–9297 (2009).
175. Firnkes, M., Pedone, D., Knezevic, J., Doblinger, M. & Rant, U. Electrically facilitated translocations of proteins through silicon nitride nanopores: conjoint and competitive action of diffusion, electrophoresis, and electroosmosis. *Nano Lett.* **10**, 2162–2167 (2010).
176. Weckman, N. E. et al. Multiplexed DNA identification using site specific dCas9 barcodes and nanopore sensing. *ACS Sens.* **4**, 2065–2072 (2019).
177. Albrecht, T. Single-molecule analysis with solid-state nanopores. *Annu. Rev. Anal. Chem.* **12**, 371–387 (2019).
178. Chuah, K. et al. Nanopore blockade sensors for ultrasensitive detection of proteins in complex biological samples. *Nat. Commun.* **10**, 2109 (2019).
179. Wang, H., Yang, R. H., Yang, L. & Tan, W. H. Nucleic acid conjugated nanomaterials for enhanced molecular recognition. *ACS Nano* **3**, 2451–2460 (2009).
180. Saha, K., Agasti, S. S., Kim, C., Li, X. N. & Rotello, V. M. Gold nanoparticles in chemical and biological sensing. *Chem. Rev.* **112**, 2739–2779 (2012).
181. Giljohann, D. A. et al. Gold nanoparticles for biology and medicine. *Angew. Chem. Int. Ed.* **49**, 3280–3294 (2010).
182. Li, S. et al. Dual-mode ultrasensitive quantification of microRNA in living cells by chiroplasmonic nanopyramids self-assembled from gold and upconversion nanoparticles. *J. Am. Chem. Soc.* **138**, 306–312 (2016).
183. Cao, Y. W. C., Jin, R. C. & Mirkin, C. A. Nanoparticles with Raman spectroscopic fingerprints for DNA and RNA detection. *Science* **297**, 1536–1540 (2002).
184. Nath, N. & Chilkoti, A. Label-free biosensing by surface plasmon resonance of nanoparticles on glass: optimization of nanoparticle size. *Anal. Chem.* **76**, 5370–5378 (2004).
185. Leff, D. V., Brandt, L. & Heath, J. R. Synthesis and characterization of hydrophobic, organically-soluble gold nanocrystals functionalized with primary amines. *Langmuir* **12**, 4723–4730 (1996).
186. Jana, N. R., Earhart, C. & Ying, J. Y. Synthesis of water-soluble and functionalized nanoparticles by silica coating. *Chem. Mater.* **19**, 5074–5082 (2007).
187. Blundell, E., Vogel, R. & Platt, M. Particle-by-particle charge analysis of DNA-modified nanoparticles using tunable resistive pulse sensing. *Langmuir* **32**, 1082–1090 (2016).
188. Wang, H., Tang, H. R., Yang, C. & Li, Y. X. Selective single molecule nanopore sensing of microRNA using PNA functionalized magnetic core-shell Fe3O4-Au nanoparticles. *Anal. Chem.* **91**, 7965–7970 (2019).
189. Ang, Y. S. & Yung, L.-Y. L. Rapid and label-free single-nucleotide discrimination via an integrative nanoparticle–nanopore approach. *ACS Nano* **6**, 8815–8823 (2012).
190. Karhanek, M., Kemp, J. T., Pourmand, N., Davis, R. W. & Webb, C. D. Single DNA molecule detection using nanopipettes and nanoparticles. *Nano Lett.* **5**, 403–407 (2005).
191. Wang, Y. X. et al. Resistive-pulse measurements with nanopipettes: detection of Au nanoparticles and nanoparticle-bound anti-peanut IgY. *Chem. Sci.* **4**, 655–663 (2013).
192. Cai, H. et al. Resistive-pulse measurements with nanopipettes: detection of vascular endothelial growth factor C (VEGF-C) using antibody-decorated nanoparticles. *Anal. Chem.* **87**, 6403–6410 (2015).
193. Wu, X. L. et al. Unexpected chirality of nanoparticle dimers and ultrasensitive chiroplasmonic bioanalysis. *J. Am. Chem. Soc.* **135**, 18629–18636 (2013).
194. Yeo, W. H. et al. Dielectrophoretic concentration of low-abundance nanoparticles using a nanostructured tip. *Nanotechnology* **23**, 485707 (2012).
195. Paulose Nadappuram, B et al. Nanoscale tweezers for single-cell biopsies. *Nat. Nanotechnol.* **14**, 80–88 (2019).
196. Squires, A., Atas, E. & Meller, A. Nanopore sensing of individual transcription factors bound to DNA. *Sci. Rep.* **5**, 11643 (2015).
197. Japrung, D. et al. SSB binding to single-stranded DNA probed using solid-state nanopore sensors. *J. Phys. Chem. B* **118**, 11605–11612 (2014).
198. Yu, J. S. et al. Identifying the location of a single protein along the DNA strand using solid-state nanopores. *ACS Nano* **9**, 5289–5298 (2015).
199. Bell, N. A. W. & Keyser, U. F. Specific protein detection using designed DNA carriers and nanopores. *J. Am. Chem. Soc.* **137**, 2035–2041 (2015).
200. Nivala, J., Marks, D. B. & Akeson, M. Unfoldase-mediated protein translocation through an alpha-hemolysin nanopore. *Nat. Biotechnol.* **31**, 247–250 (2013).
201. Wloka, C. et al. Label-free and real-time detection of protein ubiquitination with a biological nanopore. *ACS Nano* **11**, 4387–4394 (2017).
202. Loh, A. Y. Y. et al. Electric single-molecule hybridization detector for short DNA fragments. *Anal. Chem.* **90**, 14063–14071 (2018).
203. Chen, K. K. et al. Digital data storage using DNA nanostructures and solid-state nanopores. *Nano Lett.* **19**, 1210–1215 (2019).
204. Ketterer, P. et al. DNA origami scaffold for studying intrinsically disordered proteins of the nuclear pore complex. *Nat. Commun.* **9**, 902 (2018).
205. Tian, K., He, Z. J., Wang, Y., Chen, S. J. & Gu, L. Q. Designing a polycationic probe for simultaneous enrichment and detection of MicroRNAs in a nanopore. *ACS Nano* **7**, 3962–3969 (2013).
206. Xi, D. M. et al. Nanopore-based selective discrimination of microRNAs with single-nucleotide difference using locked nucleic acid-modified probes. *Anal. Chem.* **88**, 10540–10546 (2016).
207. Tian, K., Decker, K., Aksimentiev, A. & Gu, L. Q. Interference-free detection of genetic biomarkers using synthetic dipole-facilitated nanopore dielectrophoresis. *ACS Nano* **11**, 1204–1213 (2017).
208. Ying, Y. L., Wang, H. Y., Sutherland, T. C. & Long, Y. T. Monitoring of an ATP-binding aptamer and its conformational changes using an alpha-hemolysin nanopore. *Small* **7**, 87–94 (2011).
209. Restrepo-Perez, L. et al. Resolving chemical modifications to a single amino acid within a peptide using a biological nanopore. *ACS Nano* **13**, 13668–13676 (2019).
210. Gershow, M. & Golovchenko, J. A. Recapturing and trapping single molecules with a solid-state nanopore. *Nat. Nanotechnol.* **2**, 775–779 (2007).
211. Langecker, M., Pedone, D., Simmel, F. C. & Rant, U. Electrophoretic time-of-flight measurements of single DNA molecules with two stacked nanopores. *Nano Lett.* **11**, 5002–5007 (2011).
212. Pud, S. et al. Mechanical trapping of DNA in a double-nanopore system. *Nano Lett.* **16**, 8021–8028 (2016).
213. Liu, X., Zhang, Y. N., Nagel, R., Reisner, W. & Dunbar, W. B. Controlling DNA tug-of-war in a dual nanopore device. *Small* **15**, 1901704 (2019).
214. Cui, Y., Wei, Q. Q., Park, H. K. & Lieber, C. M. Nanowire nanosensors for highly sensitive and selective detection of biological and chemical species. *Science* **293**, 1289–1292 (2001).
215. Zhan, B. B. et al. Graphene field-effect transistor and its application for electronic sensing. *Small* **10**, 4042–4065 (2014).
216. Tans, S. J., Verschueren, A. R. M. & Dekker, C. Room-temperature transistor based on a single carbon nanotube. *Nature* **393**, 49–52 (1998).
217. Nakatsuka, N. et al. Aptamer–field-effect transistors overcome Debye length limitations for small-molecule sensing. *Science* **362**, 319–324 (2018).
218. Elnathan, R. et al. Biorecognition layer engineering: overcoming screening limitations of nanowire-based FET devices. *Nano Lett.* **12**, 5245–5254 (2012).
219. Gao, N. et al. Specific detection of biomolecules in physiological solutions using graphene transistor biosensors. *Proc. Natl Acad. Sci. USA* **113**, 14633–14638 (2016).
220. Patolsky, F. et al. Electrical detection of single viruses. *Proc. Natl Acad. Sci. USA* **101**, 14017–14022 (2004).
221. Panday, N. et al. Simultaneous ionic current and potential detection of nanoparticles by a multifunctional nanopipette. *ACS Nano* **10**, 11237–11248 (2016).
222. Puster, M. et al. Cross-talk between ionic and nanoribbon current signals in graphene nanoribbon-nanopore sensors for single-molecule detection. *Small* **11**, 6309–6316 (2015).
223. Graf, M., Lihter, M., Altus, D., Marion, S. & Radenovic, A. Transverse detection of DNA using a MoS_2 nanopore. *Nano Lett.* **19**, 9075–9083 (2019).
224. Nam, S. W., Rooks, M. J., Kim, K. B. & Rossnagel, S. M. Ionic field effect transistors with sub-10 nm multiple nanopores. *Nano Lett.* **9**, 2044–2048 (2009).
225. Xue, L. Nanopore-ionic field-effect transistors for selective single-molecule detection of small molecules (in the press).
226. Ren, R. et al. Selective sensing of proteins using aptamer functionalized nanopore extended field-effect transistors. *Small Methods*, 2000356 (2020).
227. Ivanov, A. R., Freedman, K. J., Kim, M. J., Albrecht, T. & Edel, J. B. High precision fabrication and positioning of nanoelectrodes in a nanopore. *ACS Nano* **8**, 1940–1948 (2014).
228. Peng, H., Rossnagel, S. M., Royyuru, A. K., Stolovitzky, G. A. & Wang, D. Fabrication of tunneling junction for nanopore DNA sequencing. US Patent 9,222,930 B2 (2015).
229. Pang, P. et al. Fixed-gap tunnel junction for reading DNA nucleotides. *ACS Nano* **8**, 11994–12003 (2014).
230. Tyagi, P. Multilayer edge molecular electronics devices: a review. *J. Mater. Chem.* **21**, 4733–4742 (2011).
231. Di Ventra, M. & Taniguchi, M. Decoding DNA, RNA and peptides with quantum tunnelling. *Nat. Nanotechnol.* **11**, 117–126 (2016).
232. Zwolak, M. & Di Ventra, M. Electronic signature of DNA nucleotides via transverse transport. *Nano Lett.* **5**, 421–424 (2005).
233. Lagerqvist, J., Zwolak, M. & Di Ventra, M. Fast DNA sequencing via transverse electronic transport. *Nano Lett.* **6**, 779–782 (2006).
234. Spinney, P. S., Collins, S. D., Howitt, D. G. & Smith, R. L. Fabrication and characterization of a solid-state nanopore with self-aligned carbon nanoelectrodes for molecular detection. *Nanotechnology* **23**, 135501 (2012).
235. Saha, K. K., Drndic, M. & Nikolic, B. K. DNA base-specific modulation of microampere transverse edge currents through a metallic graphene nanoribbon with a nanopore. *Nano Lett.* **12**, 50–55 (2012).
236. Fanget, A. et al. Nanopore integrated nanogaps for DNA detection. *Nano Lett.* **14**, 244–249 (2014).
237. Gehring, P., Thijssen, J. M. & van der Zant, H. S. J. Single-molecule quantum-transport phenomena in break junctions. *Nat. Rev. Phys.* **1**, 381–396 (2019).
238. Xiang, D., Jeong, H., Lee, T. & Mayer, D. Mechanically controllable break junctions for molecular electronics. *Adv. Mater.* **25**, 4845–4867 (2013).
239. Thomas, J. O. et al. Understanding resonant charge transport through weakly coupled single-molecule junctions. *Nat. Commun.* **10**, 4628 (2019).
240. Puczkarski, P. et al. Low-frequency noise in graphene tunnel junctions. *ACS Nano* **12**, 9451–9460 (2018).
241. Xiang, J. et al. A controllable electrochemical fabrication of metallic electrodes with a nanometer/angstrom-sized gap using an electric double layer as feedback. *Angew. Chem. Int. Ed.* **44**, 1265–1268 (2005).
242. Li, C. Z., He, H. X. & Tao, N. J. Quantized tunneling current in the metallic nanogaps formed by electrodeposition and etching. *Appl. Phys. Lett.* **77**, 3995–3997 (2000).
243. Heerema, S. J. & Dekker, C. Graphene nanodevices for DNA sequencing. *Nat. Nanotechnol.* **11**, 127–136 (2016).
244. Farimani, A. B., Min, K. & Aluru, N. R. DNA base detection using a single-layer MoS_2. *ACS Nano* **8**, 7914–7922 (2014).

245. Zhang, B. T. et al. Observation of giant conductance fluctuations in a protein. *Nano Futures* **1**, 035002 (2017).
246. Zhang, B. T. & Lindsay, S. Electronic decay length in a protein molecule. *Nano Lett.* **19**, 4017–4022 (2019).
247. Im, J., Sen, S., Lindsay, S. & Zhang, P. M. Recognition tunneling of canonical and modified RNA nucleotides for their identification with the aid of machine learning. *ACS Nano* **12**, 7067–7075 (2018).
248. Lindsay, S. et al. Recognition tunneling. *Nanotechnology* **21**, 262001 (2010).
249. Gilboa, T. & Meller, A. Optical sensing and analyte manipulation in solid-state nanopores. *Analyst* **140**, 4733–4747 (2015).
250. Spitzberg, J. D., Zrehen, A., van Kooten, X. F. & Meller, A. Plasmonic-nanopore biosensors for superior single-molecule detection. *Adv. Mater.* **31**, 1900422 (2019).
251. Garoli, D., Yamazaki, H., Maccaferri, N. & Wanunu, M. Plasmonic nanopores for single-molecule detection and manipulation: toward sequencing applications. *Nano Lett.* **19**, 7553–7562 (2019).
252. Dahlin, A. B. Sensing applications based on plasmonic nanopores: the hole story. *Analyst* **140**, 4748–4759 (2015).
253. Miller, A. E. et al. Single-molecule dynamics of phytochrome-bound fluorophores probed by fluorescence correlation spectroscopy. *Proc. Natl Acad. Sci USA* **103**, 11136–11141 (2006).
254. Chen, P. et al. Probing single DNA molecule transport using fabricated nanopores. *Nano Lett.* **4**, 2293–2298 (2004).
255. Ito, T., Sun, L. & Crooks, R. M. Observation of DNA transport through a single carbon nanotube channel using fluorescence microscopy. Chem. Commun., 1482-1483 (2003).
256. Nykypanchuk, D., Strey, H. H. & Hoagland, D. A. Brownian motion of DNA confined within a two-dimensional array. *Science* **297**, 987–990 (2002).
257. Mannion, J. T., Reccius, C. H., Cross, J. D. & Craighead, H. G. Conformational analysis of single DNA molecules undergoing entropically induced motion in nanochannels. *Biophys. J.* **90**, 4538–4545 (2006).
258. Chansin, G. A. et al. Single-molecule spectroscopy using nanoporous membranes. *Nano Lett.* **7**, 2901–2906 (2007).
259. Chansin, G. A. T. et al. Resizing metal-coated nanopores using a scanning electron microscope. *Small* **7**, 2736–2741 (2011).
260. Freedman, K. J. et al. Nanopore sensing at ultra-low concentrations using single-molecule dielectrophoretic trapping. *Nat. Commun.* **7**, 10217 (2016).
261. Ando, G., Hyun, C., Li, J. & Mitsui, T. Directly observing the motion of DNA molecules near solid-state nanopores. *ACS Nano* **6**, 10090–10097 (2012).
262. Yamazaki, H., Mizuguchi, T., Esashika, K. & Saiki, T. Electro-osmotic trapping and compression of single DNA molecules while passing through a nanopore. *Analyst* **144**, 5381–5388 (2019).
263. Auger, T. et al. Zero-mode waveguide detection of flow-driven DNA translocation through nanopores. *Phys. Rev. Lett.* **113**, 028302 (2014).
264. Yamazaki, H., Esashika, K. & Saiki, T. A 150 nm ultraviolet excitation volume on a porous silicon membrane for direct optical observation of DNA coil relaxation during capture into nanopores. *Nano Futures* **1**, 011001 (2017).
265. Assad, O. N., Di Fiori, N., Squires, A. H. & Meller, A. Two color DNA barcode detection in photoluminescence suppressed silicon nitride nanopores. *Nano Lett.* **15**, 745–752 (2015).
266. Assad, O. N. et al. Light-enhancing plasmonic-nanopore biosensor for superior single-molecule detection. *Adv. Mater.* **29**, 1605442 (2017).
267. Soni, G. V. et al. Synchronous optical and electrical detection of biomolecules traversing through solid-state nanopores. *Rev. Sci. Instrum.* **81**, 014301 (2010).
268. McNally, B. et al. Optical recognition of converted DNA nucleotides for single-molecule DNA sequencing using nanopore arrays. *Nano Lett.* **10**, 2237–2244 (2010).
269. Eid, J. et al. Real-time DNA sequencing from single polymerase molecules. *Science* **323**, 133–138 (2009).
270. Larkin, J., Foquet, M., Turner, S. W., Korlach, J. & Wanunu, M. Reversible positioning of single molecules inside zero-mode waveguides. *Nano Lett.* **14**, 6023–6029 (2014).
271. Gilboa, T. et al. Single-molecule DNA methylation quantification using electro-optical sensing in solid-state nanopores. *ACS Nano* **10**, 8861–8870 (2016).
272. Sawafta, F., Clancy, B., Carlsen, A. T., Huber, M. & Hall, A. R. Solid-state nanopores and nanopore arrays optimized for optical detection. *Nanoscale* **6**, 6991–6996 (2014).
273. Roelen, Z., Bustamante, J. A., Carlsen, A., Baker-Murray, A. & Tabard-Cossa, V. Instrumentation for low noise nanopore-based ionic current recording under laser illumination. *Rev. Sci. Instrum.* **89**, 015007 (2018).
274. Ivankin, A. et al. Label-free optical detection of biomolecular translocation through nanopore arrays. *ACS Nano* **8**, 10774–10781 (2014).
275. Anderson, B. N. et al. Probing solid-state nanopores with light for the detection of unlabeled analytes. *ACS Nano* **8**, 11836–11845 (2014).
276. Wang, Y. et al. Fabrication of multiple nanopores in a SiNx membrane via controlled breakdown. *Sci. Rep.* **8**, 1234 (2018).
277. Zrehen, A., Gilboa, T. & Meller, A. Real-time visualization and sub-diffraction limit localization of nanometer-scale pore formation by dielectric breakdown. *Nanoscale* **9**, 16437–16445 (2017).
278. Gilboa, T., Zvuloni, E., Zrehen, A., Squires, A. H. & Meller, A. Automated, ultra-fast laser-drilling of nanometer scale pores and nanopore arrays in aqueous solutions. *Adv. Funct. Mater.* **30**, 1900642 (2019).
279. Carter, K. P., Young, A. M. & Palmer, A. E. Fluorescent sensors for measuring metal ions in living systems. *Chem. Rev.* **114**, 4564–4601 (2014).
280. Heron, A. J., Thompson, J. R., Mason, A. E. & Wallace, M. I. Direct detection of membrane channels from gels using water-in-oil droplet bilayers. *J. Am. Chem. Soc.* **129**, 16042–16047 (2007).
281. Heron, A. J., Thompson, J. R., Cronin, B., Bayley, H. & Wallace, M. I. Simultaneous measurement of ionic current and fluorescence from single protein pores. *J. Am. Chem. Soc.* **131**, 1652–1653 (2009).
282. Wang, Y. et al. Osmosis-driven motion-type modulation of biological nanopores for parallel optical nucleic acid sensing. *ACS Appl. Mater. Interfaces* **10**, 7788–7797 (2018).
283. Wang, Y. et al. Electrode-free nanopore sensing by DiffusiOptoPhysiology. *Sci. Adv.* **5**, eaar3309 (2019).
284. Jonsson, M. P. & Dekker, C. Plasmonic nanopore for electrical profiling of optical intensity landscapes. *Nano Lett.* **13**, 1029–1033 (2013).
285. Reiner, J. E. et al. Temperature sculpting in yoctoliter volumes. *J. Am. Chem. Soc.* **135**, 3087–3094 (2013).
286. Crick, C. R. et al. Precise attoliter temperature control of nanopore sensors using a nanoplasmonic bullseye. *Nano Lett.* **15**, 553–559 (2015).
287. Crick, C. R. et al. Low-noise plasmonic nanopore biosensors for single molecule detection at elevated temperatures. *ACS Photonics* **4**, 2835–2842 (2017).
288. Li, Y. et al. Asymmetric plasmonic induced ionic noise in metallic nanopores. *Nanoscale* **8**, 12324–12329 (2016).
289. Zhu, W. et al. Quantum mechanical effects in plasmonic structures with subnanometre gaps. *Nat. Commun.* **7**, 11495 (2016).
290. Shi, X. et al. An integrated system for optical and electrical detection of single molecules/particles inside a solid-state nanopore. *Faraday Discuss.* **184**, 85–99 (2015).
291. Verschueren, D. V. et al. Label-free optical detection of DNA translocations through plasmonic nanopores. *ACS Nano* **13**, 61–70 (2019).
292. Shi, X., Verschueren, D. V. & Dekker, C. Active delivery of single DNA molecules into a plasmonic nanopore for label-free optical sensing. *Nano Lett.* **18**, 8003–8010 (2018).
293. Shi, X. et al. A scattering nanopore for single nanoentity sensing. *ACS Sens.* **1**, 1086–1090 (2016).
294. Kerman, S. et al. Raman fingerprinting of single dielectric nanoparticles in plasmonic nanopores. *Nanoscale* **7**, 18612–18618 (2015).
295. Chen, C. et al. High spatial resolution nanoslit SERS for single-molecule nucleobase sensing. *Nat. Commun.* **9**, 1733 (2018).
296. Huang, J.-A. et al. Single-molecule DNA bases discrimination in oligonucleotides by controllable trapping in plasmonic nanoholes. *Nat. Commun.* **10**, 5321 (2019).
297. Cecchini, M. P. et al. Rapid ultrasensitive single particle surface-enhanced Raman spectroscopy using metallic nanopores. *Nano Lett.* **13**, 4602–4609 (2013).
298. Freedman, K. J. et al. On-demand surface- and tip-enhanced Raman spectroscopy using dielectrophoretic trapping and nanopore sensing. *ACS Photonics* **3**, 1036–1044 (2016).
299. Ohayon, S., Girsault, A., Nasser, M., Shen-Orr, S. & Meller, A. Simulation of single-protein nanopore sensing shows feasibility for whole-proteome identification. *PLoS Comput. Biol.* **15**, e1007067 (2019).
300. Nicoli, F., Verschueren, D., Klein, M., Dekker, C. & Jonsson, M. P. DNA translocations through solid-state plasmonic nanopores. *Nano Lett.* **14**, 6917–6925 (2014).
301. Yamazaki, H. et al. Label-free single-molecule thermoscopy using a laser-heated nanopore. *Nano Lett.* **17**, 7067–7074 (2017).
302. Zhang, M. et al. Thermophoresis-controlled size-dependent DNA translocation through an array of nanopores. *ACS Nano* **12**, 4574–4582 (2018).
303. Verschueren, D., Shi, X. & Dekker, C. Nano-optical tweezing of single proteins in plasmonic nanopores. *Small Methods* **3**, 1800465 (2019).
304. Kotsifaki, D. & Nic Chormaic, S. Plasmonic optical tweezers based on nanostructures: fundamentals, advances and prospects. *Nanophotonics* **8**, 1227–1245 (2019).
305. Garoli, D. et al. Hybrid plasmonic nanostructures based on controlled integration of MoS_2 flakes on metallic nanoholes. *Nanoscale* **10**, 17105–17111 (2018).
306. Im, H., Wittenberg, N. J., Lesuffleur, A., Lindquist, N. C. & Oh, S.-H. Membrane protein biosensing with plasmonic nanopore arrays and pore-spanning lipid membranes. *Chem. Sci.* **1**, 688–696 (2010).
307. Liu, Q. et al. Detection of DNA base modifications by deep recurrent neural network on Oxford Nanopore sequencing data. *Nat. Commun.* **10**, 2449 (2019).
308. Nivala, J., Mulroney, L., Li, G., Schreiber, J. & Akeson, M. Discrimination among protein variants using an unfoldase-coupled nanopore. *ACS Nano* **8**, 12365–12375 (2014).
309. Cardozo, N. et al. Multiplexed direct detection of barcoded protein reporters on a nanopore array. Preprint at. *bioRxiv* https://doi.org/10.1101/837542 (2019).
310. Misiunas, K., Ermann, N. & Keyser, U. F. QuipuNet: convolutional neural network for single-molecule nanopore sensing. *Nano Lett.* **18**, 4040–4045 (2018).
311. Im, J., Lindsay, S., Wang, X. & Zhang, P. M. Single molecule identification and quantification of glycosaminoglycans using solid-state nanopores. *ACS Nano* **13**, 6308–6318 (2019).
312. Henley, R. Y. et al. Electrophoretic deformation of individual transfer RNA molecules reveals their identity. *Nano Lett.* **16**, 138–144 (2016).
313. Wei, Z. X. et al. Learning shapelets for improving single-molecule nanopore sensing. *Anal. Chem.* **91**, 10033–10039 (2019).
314. Yanagi, I., Akahori, R. & Takeda, K.-I. Stable fabrication of a large nanopore by controlled dielectric breakdown in a high-pH solution for the detection of various-sized molecules. *Sci. Rep.* **9**, 13143 (2019).
315. Storm, A. J. et al. Fast DNA translocation through a solid-state nanopore. *Nano Lett.* **5**, 1193–1197 (2005).
316. Shin, J. W., Lee, J. Y., Oh, D. H., Kim, T. W. & Cho, W. J. Shrinkage and expansion mechanisms of SiO_2 elliptical membrane nanopores. *Appl. Phys. Lett.* **93**, 221903 (2008).
317. Carson, S., Wilson, J., Aksimentiev, A. & Wanunu, M. Smooth DNA transport through a narrowed pore geometry. *Biophys. J.* **107**, 2381–2393 (2014).
318. Langecker, M. et al. Nanopores suggest a negligible influence of CpG methylation on nucleosome packaging and stability. *Nano Lett.* **15**, 783–790 (2015).
319. Waduge, P. et al. Nanopore-based measurements of protein size, fluctuations, and conformational changes. *ACS Nano* **11**, 5706–5716 (2017).
320. Hu, R. et al. Differential enzyme flexibility probed using solid-state nanopores. *ACS Nano* **12**, 4494–4502 (2018).
321. Yu, J.-S. et al. Differentiation of selectively labeled peptides using solid-state nanopores. *Nanoscale* **11**, 2510–2520 (2019).
322. Fologea, D., Uplinger, J., Thomas, B., McNabb, D. S. & Li, J. Slowing DNA translocation in a solid-state nanopore. *Nano Lett.* **5**, 1734–1737 (2005).
323. Shekar, S. et al. Measurement of DNA translocation dynamics in a solid-state nanopore at 100 ns temporal resolution. *Nano Lett.* **16**, 4483–4489 (2016).
324. Carlsen, A. T., Briggs, K., Hall, A. R. & Tabard-Cossa, V. Solid-state nanopore localization by controlled breakdown of selectively thinned membranes. *Nanotechnology* **28**, 085304 (2017).

325. Garaj, S., Liu, S., Golovchenko, J. A. & Branton, D. Molecule-hugging graphene nanopores. *Proc. Natl Acad. Sci. USA* **110**, 12192–12196 (2013).
326. Goyal, G., Lee, Y. B., Darvish, A., Ahn, C. W. & Kim, M. J. Hydrophilic and size-controlled graphene nanopores for protein detection. *Nanotechnology* **27**, 495301 (2016).
327. Deng, Y. et al. Precise fabrication of a 5 nm graphene nanopore with a helium ion microscope for biomolecule detection. *Nanotechnology* **28**, 045302 (2016).
328. Liu, K. et al. Geometrical effect in 2D nanopores. *Nano Lett.* **17**, 4223–4230 (2017).
329. Liu, K. et al. Detecting topological variations of DNA at single-molecule level. *Nat. Commun.* **10**, 3 (2019).
330. Kim, H.-J. et al. Translocation of DNA and protein through a sequentially polymerized polyurea nanopore. *Nanoscale* **11**, 444–453 (2019).
331. Liu, L. et al. Simultaneous quantification of multiple cancer biomarkers in blood samples through DNA-assisted nanopore sensing. *Angew. Chem. Int. Ed.* **57**, 11882–11887 (2018).
332. Healey, M. J., Rowe, W., Siati, S., Sivakumaran, M. & Platt, M. Rapid assessment of site specific DNA methylation through resistive pulse sensing. *ACS Sens.* **3**, 655–660 (2018).
333. Singer, A., Rapireddy, S., Ly, D. H. & Meller, A. Electronic barcoding of a viral gene at the single-molecule level. *Nano Lett.* **12**, 1722–1728 (2012).
334. Carlsen, A. T., Zahid, O. K., Ruzicka, J. A., Taylor, E. W. & Hall, A. R. Selective detection and quantification of modified DNA with solid-state nanopores. *Nano Lett.* **14**, 5488–5492 (2014).
335. Zahid, O. K., Wang, F., Ruzicka, J. A., Taylor, E. W. & Hall, A. R. Sequence-specific recognition of microRNAs and other short nucleic acids with solid-state nanopores. *Nano Lett.* **16**, 2033–2039 (2016).
336. Kong, J., Bell, N. A. W. & Keyser, U. F. Quantifying nanomolar protein concentrations using designed DNA carriers and solid-state nanopores. *Nano Lett.* **16**, 3557–3562 (2016).
337. Beamish, E., Tabard-Cossa, V. & Godin, M. Identifying structure in short DNA scaffolds using solid-state nanopores. *ACS Sens.* **2**, 1814–1820 (2017).
338. Kong, J., Zhu, J. & Keyser, U. F. Single molecule based SNP detection using designed DNA carriers and solid-state nanopores. *Chem. Commun.* **53**, 436–439 (2017).
339. Lin, Y., Ying, Y.-L., Shi, X., Liu, S.-C. & Long, Y.-T. Direct sensing of cancer biomarkers in clinical samples with a designed nanopore. *Chem. Commun.* **53**, 11564–11567 (2017).
340. Kong, J., Zhu, J., Chen, K. & Keyser, U. F. Specific biosensing using DNA aptamers and nanopores. *Adv. Funct. Mater.* **29**, 1807555 (2019).
341. Zhao, X. et al. Translocation of tetrahedral DNA nanostructures through a solid-state nanopore. *Nanoscale* **11**, 6263–6269 (2019).
342. Thakur, M. et al. Wafer-scale fabrication of nanopore devices for single-molecule DNA biosensing using MoS_2. *Small Methods* https://doi.org/10.1002/smtd.202000072 (2020).
343. Parkin, W. M. & Drndic, M. Signal and noise in FET-nanopore devices. *ACS Sens.* **3**, 313–319 (2018).
344. Belkin, M., Chao, S.-H., Jonsson, M. P., Dekker, C. & Aksimentiev, A. Plasmonic nanopores for trapping, controlling displacement, and sequencing of DNA. *ACS Nano* **9**, 10598–10611 (2015).
345. Kesselheim, S., Muller, W. & Holm, C. Origin of current blockades in nanopore translocation experiments. *Phys. Rev. Lett.* **112**, 018101 (2014).
346. Wilson, J., Sarthak, K., Si, W., Gao, L. Y. & Aksimentiev, A. Rapid and accurate determination of nanopore ionic current using a steric exclusion model. *ACS Sens.* **4**, 634–644 (2019).

Acknowledgements
J.B.E. received funding from the European Research Council (ERC) under the European Union's Horizon 2020 research and innovation programme (grant agreement no. 724300, NanoPD and 875525, NanoPD_P). A.P.I. and J.B.E. are funded in part by BBSRC grant BB/R022429/1, EPSRC grant EP/P011985/1 and the Analytical Chemistry Trust Fund grant 600322/05. M.W. acknowledges the National Institutes of Health for support (R01 HG009186). H.Y. is a recipient of a JSPS Research Fellowship for Young Scientists (no. 20J00261) from the Japan Society for the Promotion of Science.

Author contributions
All authors contributed to the preparation of the manuscript.

Competing interests
The authors declare no competing interests.

Publisher's note
Springer Nature remains neutral with regard to jurisdictional claims in published maps and institutional affiliations.

RELATED LINKS
1991 Nobel Prize in Physiology or Medicine: https://www.nobelprize.org/prizes/medicine/1991/press-release/